CONTENTS

MULTIMEDIA CONTENTS

Figure Sources

Chapter 5. Acoustic Emission Signal Processing

Figure 1 — Vallen-Systeme GmbH, Munich, Germany.

Chapter 7. Acoustic Emission Testing for Process and Condition Monitoring

Figures 19-26 — Holroyd Instruments, Bonsall Near Matlock, Derbyshire, United Kingdom

Chapter 11. Aerospace Applications for Acoustic Emission Testing

Figures 1-11 — ASTM International, West Conshohocken, PA.

Movie Sources

Chapter 1. Introduction to Acoustic Emission Testing

Movie. Discontinuities in steel — Physical Acoustics Corporation, Princeton, NJ; for the Federal Highway Administration, United States Department of Transportation, Washington, DC.

Movie. Plastic deformation causes cry of tin — Physical Acoustics Corporation, Princeton, NJ; for the Federal Highway Administration, United States Department of Transportation, Washington, DC.

Chapter 2. Fundamentals of Acoustic Emission Testing

Movie. Acoustic emission differs from other methods — Physical Acoustics Corporation, Princeton, NJ; for the Federal Highway Administration, United States Department of Transportation, Washington, DC.

Movie. Pencil break source — Physical Acoustics Corporation, Princeton, NJ.

Movie. Guard transducers control noise — Physical Acoustics Corporation, Princeton, NJ; for the Federal Highway Administration, United States Department of Transportation, Washington, DC.

Chapter 5. Acoustic Emission Signal Processing

Movie. System with one channel — Physical Acoustics Corporation, Princeton, NJ; for the Federal Highway Administration, United States Department of Transportation, Washington, DC.

Chapter 6. Acoustic Leak Testing

Movie. Ultrasonic vibration of gas molecules escaping orifice — UE Systems, Elmsford, NY.

Sound. Audible analog of ultrasonic signal — UE Systems, Elmsford, NY.

Movie. Steam system leak test — UE Systems, Elmsford, NY.

Movie. Amplitude rise heard through ultrasound detector as rough and raspy — UE Systems, Elmsford, NY.

Chapter 7. Acoustic Emission Testing for Process and Condition Monitoring

Movie. Discontinuities from welds — Physical Acoustics Corporation, Princeton, NJ; for the Federal Highway Administration, United States Department of Transportation, Washington, DC.

Chapter 13. Acoustic Emission Testing Glossary

Movie. Pencil break source — Physical Acoustics Corporation, Princeton, NJ; for the Federal Highway Administration, United States Department of Transportation, Washington, DC.

CHAPTER 4

Acoustic Emission Source Location

Ronnie K. Miller, Loveland, Ohio

Mark F. Carlos, Physical Acoustics Corporation, Princeton, New Jersey (Part 2)

Richard D. Finlayson, Physical Acoustics Corporation, Princeton, New Jersey (Part 4)

Valery Godinez-Azcuaga, Physical Acoustics Corporation, Princeton, New Jersey (Part 4)

Matthew R. Rhodes, Physical Acoustics Corporation, Princeton, New Jersey (Part 2)

Fong Shu, Physical Acoustics Corporation, Princeton, New Jersey (Part 4)

W. David Wang, Shell Oil USA, Deer Park, Texas (Part 4)

PART 1. Fundamentals of Acoustic Emission Source Location

One of the major strengths of acoustic emission testing is its ability to locate an active source when enough data are available from one or more transducers. This ability improves the economics of techniques that may follow an acoustic emission test. The cost savings are realized with minimization of the following: (1) excavation of buried pipe during leak testing; (2) insulation removal for pressure vessel testing; (3) the time to perform the followup test (because the test becomes very localized); (4) the down time associated with out-of-service testing (because acoustic emission testing can be performed on line and so can justify leaving a vessel in service).

Baron and Ying have provided a variety of source location techniques in two categories based on whether the acoustic emission signal was continuous or discrete.[1] For each signal type, different techniques were outlined using one, two, three or more transducers.

Zone Location Technique

The basic technique using data from a single transducer is called *zone location* (Figs. 1 and 2). Assuming equal source amplitudes and transducer sensitivities, the transducer with the highest amplitude output will be closest to the source because the signal detected at the closest transducer is less attenuated. Thus, a map can be developed as in Fig. 1.

A certain degree of refinement can be achieved if, for example, it is also observed which transducer has the second highest output. Observing the second highest output reduces the zone area, as illustrated in Fig. 2. Neither this signal measurement technique nor the zone location technique will work unless the structure exhibits enough attenuation to

FIGURE 1. Zone location based solely on transducer with highest output: (a) representative one-dimensional case; (b) representative two-dimensional case.

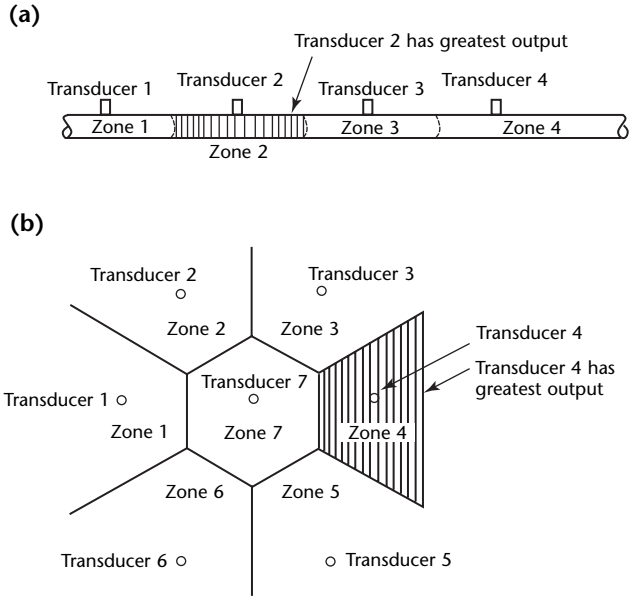

FIGURE 2. Zone location based on transducers with highest and second highest outputs: (a) representative one-dimensional case (transducer 3 has highest output; transducer 2, second highest); (b) representative two-dimensional case (transducer 3 has highest output; transducer 4, second highest).

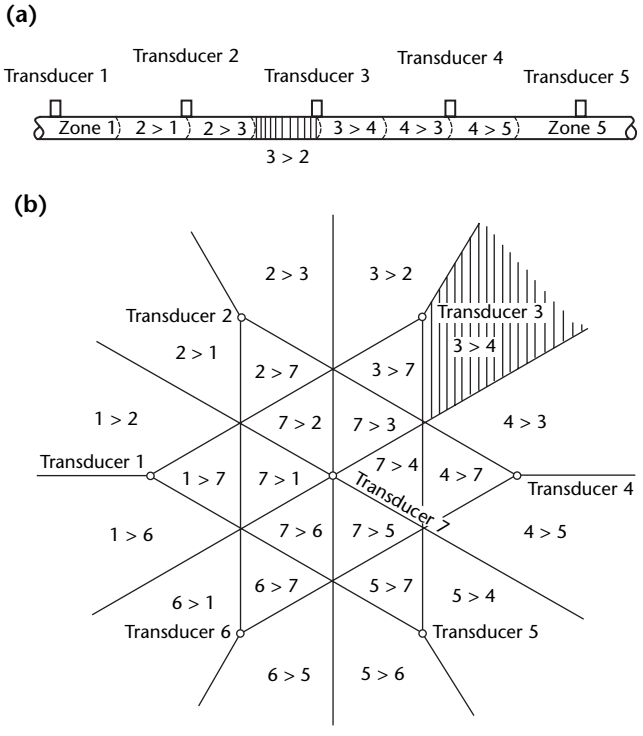

be interpreted. Similarly, the technique will not be practical if the attenuation is too severe.

This technique can be applied to discrete signals as well. In these cases, the peak amplitude of the discrete signal may be used to determine which transducer is closest to a source. An alternative (which is used more often) is to observe the sequence in which signals are detected from a given source. In some cases, where as many as three transducers detect an emission, it may be possible to define the first, second and third hit transducer and thus narrow the zone size.

Signal Amplitude Measurement (or Signal Difference) Technique

If the detailed attenuation characteristics of the structure are known, the location of the source can be computed from observation of transducer outputs. The signal amplitude measurement technique of source location comprises the three following stages, using leak location as an example.

1. Determine the two transducers closest to the leak by noting the highest and second highest outputs from the array. It is necessary that the transducer pair straddle the active source. This technique cannot be used with the situation depicted in Fig. 3, where the source is outside the array defined by the set of transducers.
2. Determine the difference (in decibels) between the two transducer outputs and compare it with the attenuation characteristics of the component.
3. On a two-dimensional plane, this process describes a hyperbola passing through the leak site. (This approach is equivalent to using Δt measurements to locate a transient source.) A similar process is undertaken using at least one other transducer to generate an intersecting hyperbola. The intersection of the hyperbolae defines the source (equivalent to two-dimensional source location of transient signals using time difference measurements).

The following example illustrates the process for a one-dimensional case. Consider a gas filled steel pipe, 150 mm (6 in.) in diameter and 84 m (275 ft) long. The attenuation characteristics are as illustrated in Fig. 4.[2] It has been determined that 100 kHz transducers will be used and positioned so that attenuation between transducers will not exceed 25 dB. This level of attenuation occurs over 10.9 m (36 ft). A transducer spacing of 10.5 m then yields 24.3 dB attenuation between transducers. The 84 m (275 ft) long pipe will require nine transducers for complete coverage.

Now consider any transducer pair (transducer 3 and transducer 4, for example). Figure 5 and Table 1 illustrate the respective attenuation characteristics with reference to the source and transducer positions for several arbitrary leak sites. Figure 6 may then be constructed simply by subtracting the attenuation characteristic for one transducer from that of the other for a

FIGURE 3. An acoustic emission source outside of an array cannot be located by the signal amplitude measurement technique.

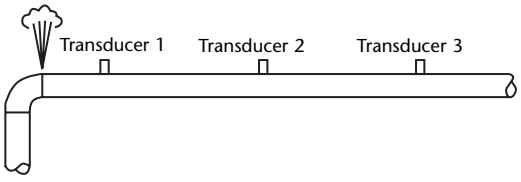

FIGURE 4. Acoustic attenuation in a 150 mm (6 in.) diameter steel pipe.

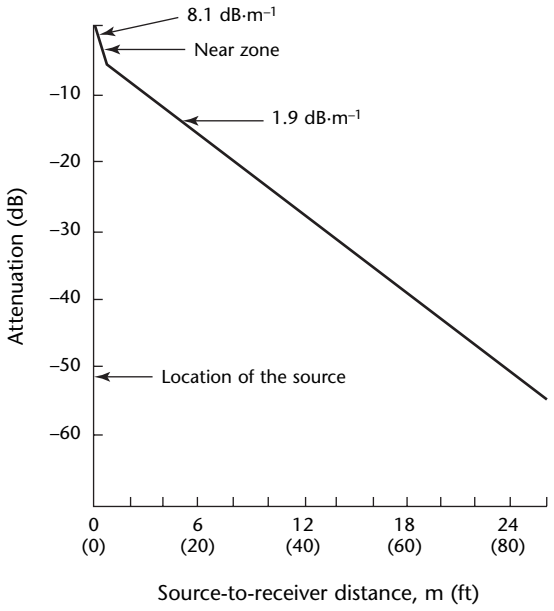

given position ($A_1 - A_2$ or $B_1 - B_2$). For a source at the midpoint between the two transducers, each transducer will display the same amplitude output; there will be zero decibels difference between the signals generated by the transducers.

TABLE 1. Signals at transducers for test with constant 200 mV noise field.

Transducer	Position m	Position (ft)	Signal True (mV)	Signal Measured (mV)
1	0	(0)	41	200
2	10.5	(413)	61	209
3	21.0	(827)	1000	1020
4	31.5	(1240)	251	321
5	42.0	(1654)	15	201
6	52.5	(2067)	1	200
7	63.0	(2480)	0	200
8	73.5	(2894)	0	200
9	84.0	(3307)	0	200

FIGURE 5. Attenuation pattern for several leak sites with a 10.5 m (34 ft) transducer separation. This chart is bounded on the left and right by the positions of transducers 3 and 4, respectively (see Table 1).

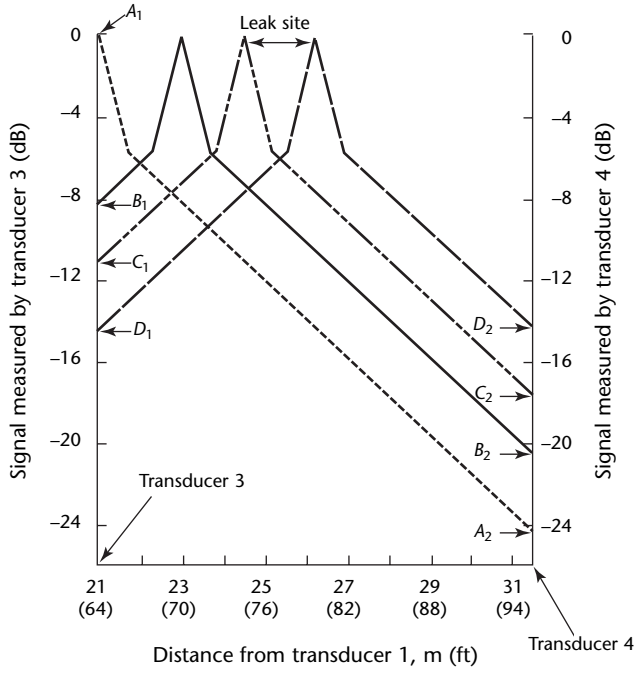

Legend

A_1, B_1, C_1, D_1 = points where signal curves from leak sites (stipulated as *A*, *B*, *C* and *D*) intersect the vertical axis at position of transducer 3

A_2, B_2, C_2, D_2 = points where signal curves from leak sites (stipulated as *A*, *B*, *C* and *D*) intersect the vertical axis at position of transducer 4

For a particular leak, if the output of transducer 3 exceeds that of transducer 4 by 12 dB, then Fig. 6 shows that the leak is located at the 23 m (76 ft) position.

This technique relies on the relative amplitude between two participating transducers. The absolute amplitudes of the transducer outputs are irrelevant. However, two assumptions are made: (1) all transducer-to-amplifier chains are adjusted to identical sensitivities; (2) ambient noise, either electronic or mechanical, is completely absent. Although it may be feasible to acceptably adjust sensitivities, it is rarely possible to eliminate noise.

In cases where noise is present, it may be necessary to measure the noise at some point where the operator is certain that there is no leak signal. With the noise level determined, the true signal level can be determined from the following:

$$\textbf{(1)} \quad S_m = \sqrt{S_t^2 + n^2}$$

where n is the root mean square of noise, S_m is the root mean square of the measured signal and S_t is the root mean square of the true signal.

In the case of discrete signals, the signal difference technique may be used as well. Especially in the case where transducer spacing is very large and the possibility of nearly simultaneous events is high, multiple signals from two or more transducers must be sorted out to determine which go together to define an event and a source location. The signal

FIGURE 6. Signal difference over distance for two transducers.

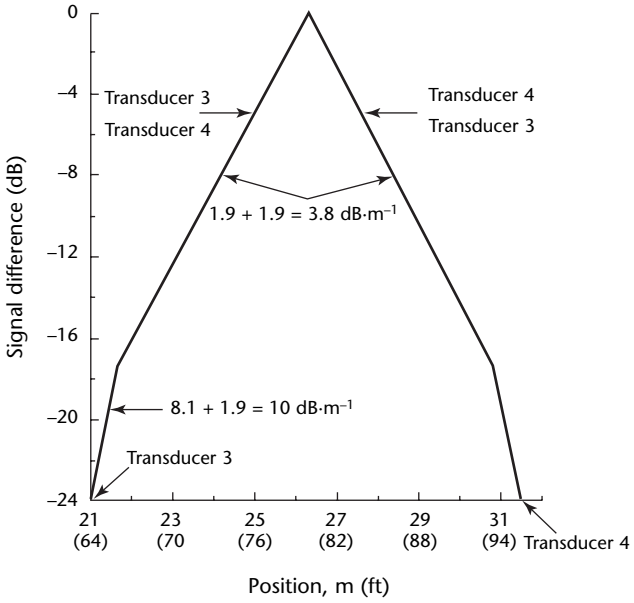

difference can be measured and compared with an attenuation model to determine if the right signals have been chosen for defining the event.

Timing Technique

When acoustic emission signals are transient (have a well defined beginning and end), it is much more apparent that timing techniques can form the basis of a useful source location methodology. If it is possible to identify a particular characteristic of the signal as it is detected by a transducer array, then timing techniques can be used.

The technique develops the time delay of a particular signal between two or more transducers. This procedure may provide the position of the source but it can also be the result of different wave paths, different wave modes or dispersion. This confusion is analogous to the problems encountered in burst emission source location.

It is necessary to first determine a true sound velocity or this technique can be particularly difficult, for example, on piping. It should be emphasized that timing techniques are not necessarily more problematic than attenuation measurement. Fortunately, both sound attenuation and velocity can be accurately measured even in a complex structure, so that both source location techniques may often be used successfully.

Cross Correlation Approach

Conventional techniques for measuring time differences between two burst type acoustic emission waves cannot be used for continuous sources such as leaks. However, cross correlation techniques can be used to measure the time difference or time delay of one wave from another for both discrete waves and continuous waves.[3] The technique has been effectively used in acoustic emission testing.[4] Cross correlation techniques have proved particularly useful in locating leak sites on pipes.[5]

For practical applications, the cross correlation function between an arbitrary wave $A(t)$ and another wave $B(t + \tau)$ with a time delay τ (second) is given by:

$$\textbf{(2)} \qquad R_{AB}(\tau) = \frac{1}{T}\int_0^T A(t)B(t+\tau)dt$$

where T is a finite time interval (second). This definition is different from the general definition, in which T approaches infinity. A finite time interval allows practical applications of the technique. Other reasons for using a finite time interval are discussed below.

Equation 2 requires that the product of $A(t)$ and $B(t + \tau)$ be integrated over time t. Then, if τ is considered a variable, the cross correlation function $R_{AB}(\tau)$ is a function of τ. In other words, for a given τ_j, $R_{AB}(\tau_j)$ is obtained from the integration of $A(t)B(t)$. The characteristics of $R_{AB}(\tau)$ become clear if $R_{AB}(\tau)$ is generated with the following procedure: let $A(t)$ and $B(t)$ be divided for n small and equal time intervals.

When $t = t_i$, then $A(t) = a_i$, $B(t) = b_i$ and $i = 0, 1, 2 \ldots n$, if $B(t)$ has a time delay τ' with respect to $A(t)$. Then, when $j = 0, 1, 2 \ldots n$:

$$\textbf{(3)} \qquad R_{AB}(\tau_j) = \sum_{i=0}^{n} a_{i+j}\, b_i$$

or when $j = -1, -2, \ldots -n$:

$$\textbf{(4)} \qquad R_{AB}(\tau_j) = \sum_{i=0}^{n} a_i\, b_{i-j}$$

and when $j = 0$:

$$\textbf{(5)} \qquad d = \frac{1}{2}(D - \Delta tV)$$

The subscripts of a_{i+j} and b_{i-j} in Eq. 3 shift relatively in accordance with the shift of τ_j for $R_{AB}(\tau_j)$.

The cross correlation function is an integration over a finite time period. Furthermore, in practical applications, a finite portion of each wave is used for data sampling and the wave amplitude beyond the portion used is equal to zero ($a_i = b_i = 0$, if $i > n$).

Therefore, if $j > 0$ and $i + j > n$, then $a_{i+j} = 0$; and if $j < 0$ and $i - j > n$, then $b_{i-j} = 0$. Stated otherwise, when $|j|$ increases, then $i + j$ increases and some of the summation terms in Eq. 3 become zero. Therefore, as $|j|$ increases, the number of summation terms diminishes and the amplitude of $R_{AB}(\tau_j)$ decreases. Finally, when $|j| > n$, all a_{i+j} and b_{i-j} are equal to zero so that $R_{AB}(\tau_j) = 0$. When $\tau_j = \tau'$, then $R_{AB}(\tau')$ reaches the maximum value because A and B become in phase. From the maximum peak of $R_{AB}(\tau_j)$, the time difference or time delay τ' of $B(t)$ from $A(t)$ is obtained.

The following example illustrates the calculation procedure and the characteristics of the cross correlation function. Assume $A(t)$ and $B(t)$ are sinusoidal functions so that

$A(t) = A_0 \sin \omega t$ and
$B(t) = B_0 \sin [\omega t - (\pi \div 6)]$.

For simplicity, assume $A_0 = B_0 = 1$. As shown in Figs. 7a and 7b, the ωt axes of both $A(t)$ and $B(t)$ are divided into twelve equal intervals, corresponding to $A(t) = a_0, a_1, a_2 \ldots a_{12}$ and $B(t) = b_0, b_1, b_2 \ldots b_{12}$. Then, using Eq. 3, the cross correlation function is calculated at $j = -12, -11 \ldots 0 \ldots 11, 12$. The results are plotted in Fig. 7c.

As shown in Fig. 7c, when $\omega\tau = \omega\tau_{-1} = -\pi \div 6$, then $R_{AB}(\tau_{-1})$ is maximum. As $\omega\tau$ increases, the absolute values of the $R_{AB}(\tau)$ peaks decrease. When $-2\pi \geq \omega\tau \geq 2\pi$, then $R_{AB}(\tau) = 0$. This example illustrates the characteristics of a cross correlation function in a finite time interval. Note that, if the integration time interval approaches infinity, the cross correlation function $R_{AB}(\tau)$ becomes a continuous cosine wave with no distinguishable maximum peak value. This is the reason that a particular finite time interval is necessary for the validity of a cross correlation.

FIGURE 7. Plots of sample cross correlation function: (a) sinusoidal function $A(t)$; (b) sinusoidal function $B(t)$ with $(-\pi \div 6)$ delay; (c) cross correlation function of $A(t)$ and $B(t)$.

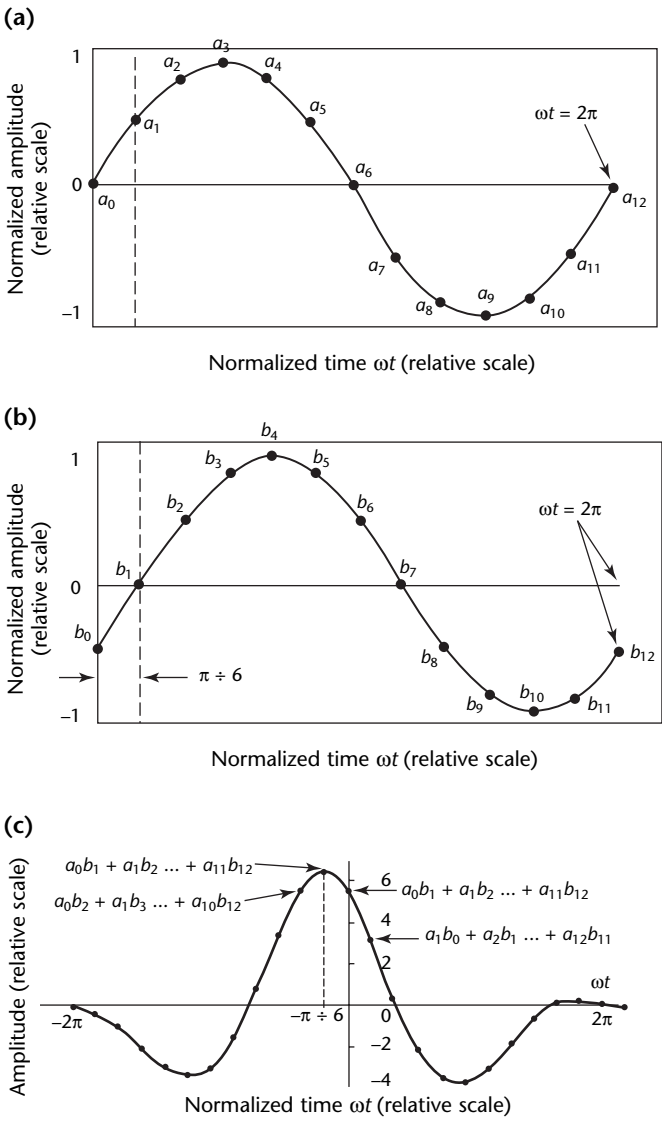

Legend

a, b = signal amplitude at time increment
t = time, normalized
τ = time delay, normalized
ω = angular frequency (rad)

Linear Location

Consider the situation where three transducers are mounted on a linear structure such as the pipe shown in Fig. 8. Assume that an acoustic emission event occurs somewhere on the pipe and that the resulting stress waves propagate in both directions at the same constant velocity. The coarsest form of source location would be to note the transducer that received the stress wave first (called the *first hit*). Referring to Fig. 8, if the first hit occurs at transducer 2, then the source lies in the area from a point halfway between transducer 1 and transducer 2 to a point halfway between transducer 2 and transducer 3. This area can be reduced

FIGURE 8. Linear source location technique on a pipe: (a) zone for first hit at transducer 2; (b) zone for first hit at transducer 2 and second hit at transducer 1; (c) hit sequence, time difference measurement $\Delta t = T_2 - T_1$; (d) source outside of array $\Delta t = T_2 - T_1 = \text{constant} \cong D$.

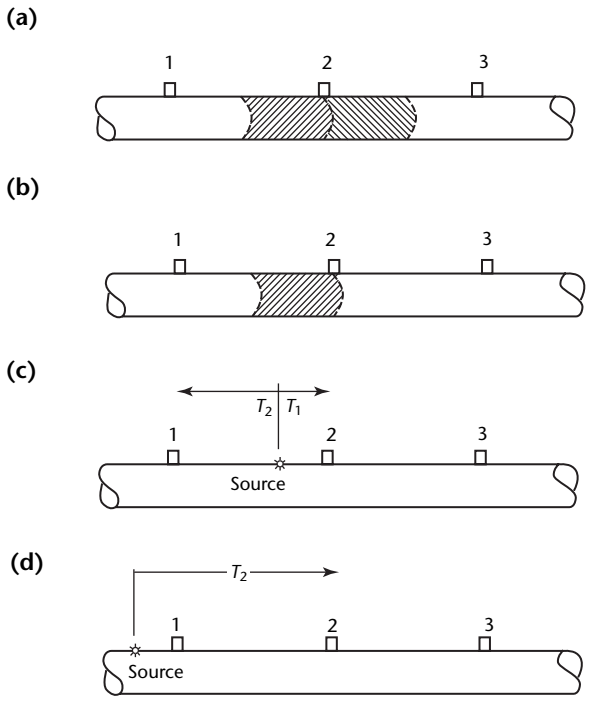

somewhat by also noting the second hit transducer. If the second hit is at transducer 1, then the source lies between transducer 2 and a point halfway between transducer 1 and transducer 2. For evenly spaced transducers, this halves the potential location zone (Fig. 8b).

This procedure is known as *zone location*. The simple input information allows only the identification of an encompassing zone rather than pinpointing the source site. However, if not only the hit sequence but the time difference between hits is measured (Fig. 8c), more precise source location can be performed. If the time difference between hits at transducer 1 and transducer 2 was zero, it would indicate a site precisely midway between the two transducers.

Or consider this situation, when the hit sequence is transducer 2 followed by transducer 1. The time difference between hits is equal to the time taken to cross the entire pair separation:

$$\textbf{(6)} \quad \Delta t = \frac{D}{V}$$

where D is the distance (meter) between transducers, V is the constant wave velocity (meter per second) and Δt is the difference (second) of arrival time.

The source would then be located at transducer 2. In general, the source location d is given by:

$$\textbf{(7)} \quad d = \frac{1}{2}\left(D - \Delta t V\right)$$

where d is measured from the first hit transducer. Note that if the source is outside of the transducer array (as in Fig. 8d), then the time difference measurement always corresponds to the time of flight between the outer transducer pair; the hit sequence remains constant. In this situation, the source is at or beyond the outer transducer.

The linear case is most appropriate when the transducer separation is large compared to the diameter of the test object. As this ratio reduces, sources close to the transducers can become mislocated if they are away from the direct axial line through the participating transducers.

Location of Sources in Two Dimensions

Consider two transducers mounted on an infinite plane and assume the ideal condition where the stress waves propagating from an acoustic emission source travel at constant velocity in all directions as shown in Fig. 9:

$$\textbf{(8)} \quad \Delta t V = r_1 - R$$

and:

$$\textbf{(9)} \quad Z = R \sin\theta$$

and:

$$\textbf{(10)} \quad Z^2 = r_1^2 - \left(D - R\cos\theta\right)^2$$

Combining Eqs. 9 and 10 gives:

$$\textbf{(11)} \quad R^2 \sin^2\theta = r_1^2 - \left(D - R\cos\theta\right)^2$$

and:

$$\textbf{(12)} \quad R^2 = r_1^2 - D^2 + 2DR\cos\theta$$

Substituting $r_1 = \Delta t V + R$ from Eq. 8 yields:

$$\textbf{(13)} \quad R = \frac{1}{2}\,\frac{D^2 - \Delta t^2 V^2}{\Delta t V + D\cos\theta}$$

Equation 13 is the equation of a hyperbola passing through the source location (X_s, Y_s). Any point on the hyperbola satisfies the input data (the hit sequence and time difference measurement).

The result illustrated in Fig. 9 is insufficient for most two-dimensional source location requirements. However, the addition of a third transducer can

FIGURE 9. Result of source location with two transducers on an infinite plane.

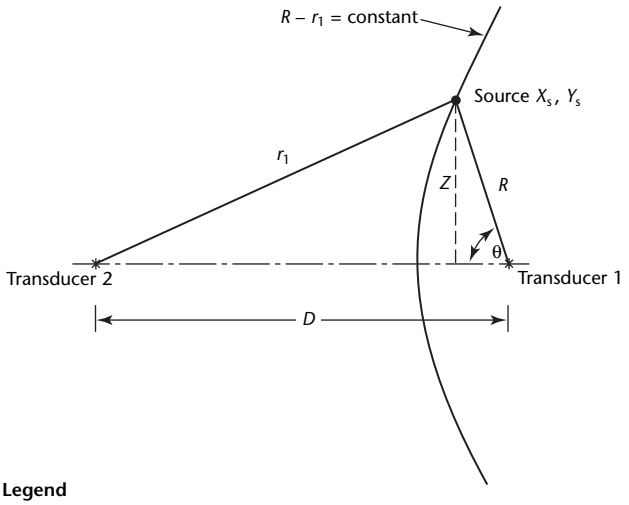

Legend

D = distance (meter) between transducers
R = distance (meter) from transducer 1 to source
r_1 = distance (meter) from transducer 2 to source
Z = distance from transducer plane to source
X_s, Y_s = cartesian coordinates for the source
θ = angle (radian)

improve the situation. The input data now include a sequence of three hits and two time difference measurements (between the first and second hit transducers and the first and third hit transducers). Figure 10 illustrates the general situation.

(14) $\Delta t_1 V = r_1 - R$

now:

(15) $\Delta t_2 V = r_2 - R$

which yields:

(16) $$R = \frac{1}{2} \frac{D_1^2 - \Delta t_1^2 V^2}{\Delta t_1 V + D_1 \cos(\theta - \theta_1)}$$

and:

(17) $$R = \frac{1}{2} \frac{D_2^2 - \Delta t_2^2 V^2}{\Delta t_2 V + D_2 \cos(\theta_3 - \theta)}$$

Equations 16 and 17 can be solved simultaneously to provide the location of a source in two dimensions as illustrated in Fig. 11 (this diagram shows an equilateral triangular array but solutions to Eqs. 16 and 17 do not require one).

FIGURE 10. Three-transducer array with detection sequence 1, 2, 3.

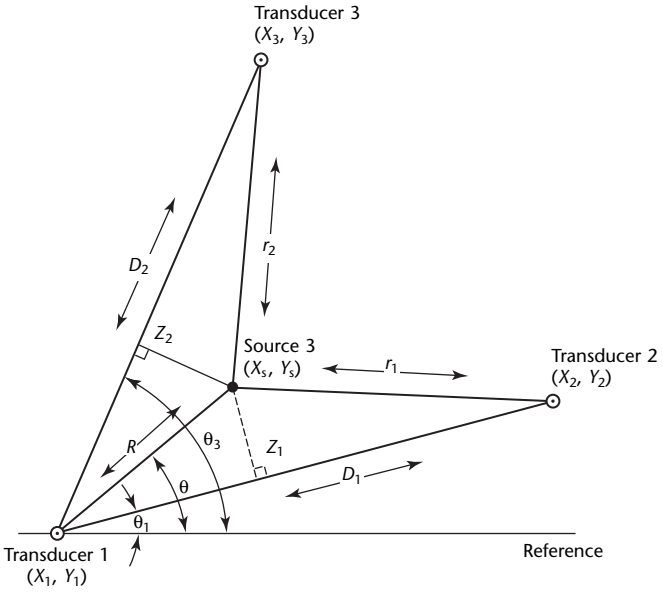

Legend

D = distance (meter) between transducers
R = distance (meter) from transducer 1 to source
r_1 = distance (meter) from transducer 2 to source
z = distance from transducer plane to source
X_s, Y_s = cartesian coordinates
θ = angle (radian)

Source Location in Three Dimensions

Most applications of acoustic emission source location techniques are directed at the problem of locating a source in a practically two-dimensional shell structure. However, when the wall is too thick or when the area of interest lies internally to the shell, then locating a source in three dimensions becomes important. In addition, there are now cases of liquid filled structures where internal sources can be located in three dimensions by using transducers mounted on the outside surface of the structure.

One approach is to extrapolate the two-dimensional technique into three dimensions. Each transducer location is defined in full spatial coordinates (X, Y and Z) and the hyperbolae of Eqs. 16 and 17 become surfaces. The solution is more involved than in two dimensions and mapping onto a two-dimensional surface presents its own set of problems.[4]

Three-Dimensional Source Location in Cylindrical Test Objects

The following approach is applicable for an intermediate (thick walled) cylindrical vessel. If the outside diameter of the cylinder is not too large, then a distribution of four transducers, as shown in Fig. 12, is sufficient for volumetrically

FIGURE 11. Intersection of hyperbolae as used for defining source position.

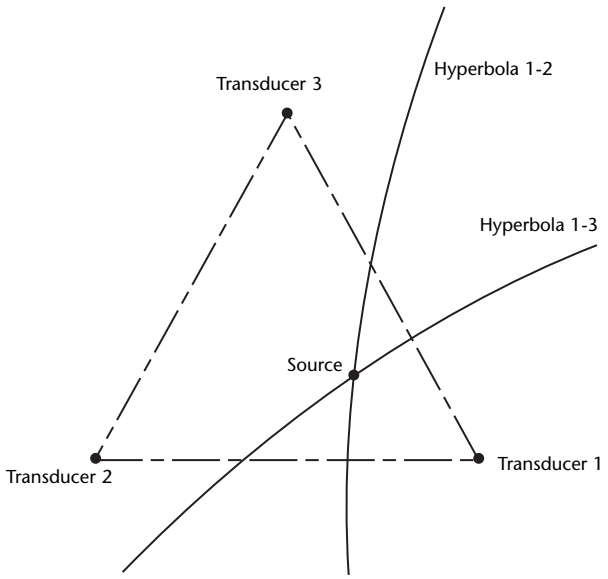

monitoring one half of the vessel. Mathematical calculations for the location of an acoustic emission source in a three-dimensional space become simpler with this arrangement.

As shown in Fig. 12, four transducers are located at (r_0, [±π ÷ 2], 0) and (r_0, 0, ±h) in cylindrical coordinates. When values of i = 1 and 2, the distance from an acoustic emission source at an arbitrary position (r, θ, z) to each transducer is:

$$\textbf{(18)} \quad d_i = \sqrt{z^2 + a_i^2}$$

where:

$$\textbf{(19)} \quad a_1^2 = r_0^2 + r^2 + 2r_0 r \sin\theta$$

and:

$$\textbf{(20)} \quad a_2^2 = r_0^2 + r^2 + 2r_0 r \sin\theta$$

For i = 3 and 4, the distance from an acoustic emission source at an arbitrary position (r, θ, z) to each transducer is:

$$\textbf{(21)} \quad d_i = \sqrt{(h \pm z)^2 + a_i^2}$$

where $a_3^2 = a_4^2$ and $a_3^2 = r_0^2 + r^2 - 2r_0 r \cos\theta$. When j = 1, 2, 3 and 4 and the subscripts i and j indicate transducer numbers, then:

$$\textbf{(22)} \quad d_i + d_j = v\Delta t_{ij}$$

The basic relations in Eqs. 18 to 22 lead to a quadratic equation for z in terms of r and θ for each pair of transducers. The solution of the quadratic equation for transducer 1 and transducer 2 is:

$$\textbf{(23)} \quad z = \left(\frac{4r_0^2 r^2 \sin^2\theta}{v^2 \Delta t_{12}^2} + \frac{1}{4} v^2 \Delta t_{12}^2 - r_0^2 - r^2 \right)^{0.5}$$

For transducer 1 and transducer 3:

$$\textbf{(24)} \quad z = \frac{-B \pm \sqrt{B^2 - 4AC}}{2A}$$

Equations 25 to 27 define the terms used in Eq. 24:

$$\textbf{(25)} \quad A = 4\left(h^2 - v^2 \Delta t_{13}^2\right)$$

$$\textbf{(26)} \quad B = 4hr_0 r\left(2\cos\theta - \sin\theta\right) - hA$$

$$\textbf{(27)} \quad C = 4r_0^2 r^2 \left(\cos\theta - \sin\theta\right)^2 + v^4 \Delta t_{13}^4 - 4v^2 \Delta t_{13}^2 \left(r_0^2 + r^2\right) + 4r_0 r \left(\cos\theta + \sin\theta\right) v^2 \Delta t_{13}^2 - 2h^2 v^2 \Delta t_{13}^2 + 2h^2 r_0 r \left(\sin\theta + 2\cos\theta\right) + h^4$$

To make Eq. 24 valid for transducer 1 and transducer 4, h and Δt_{13} in Eqs. 25 to 27 should be replaced by $-h$ and Δt_{14}, respectively.

The purpose for the development of Eqs. 23 and 24 is to simplify computer programming. Both equations can be used to calculate values of z for each pair of transducers from given values of r and θ. Therefore, all possible solutions for z can

FIGURE 12. Source location in three dimensions for thick walled cylinder.

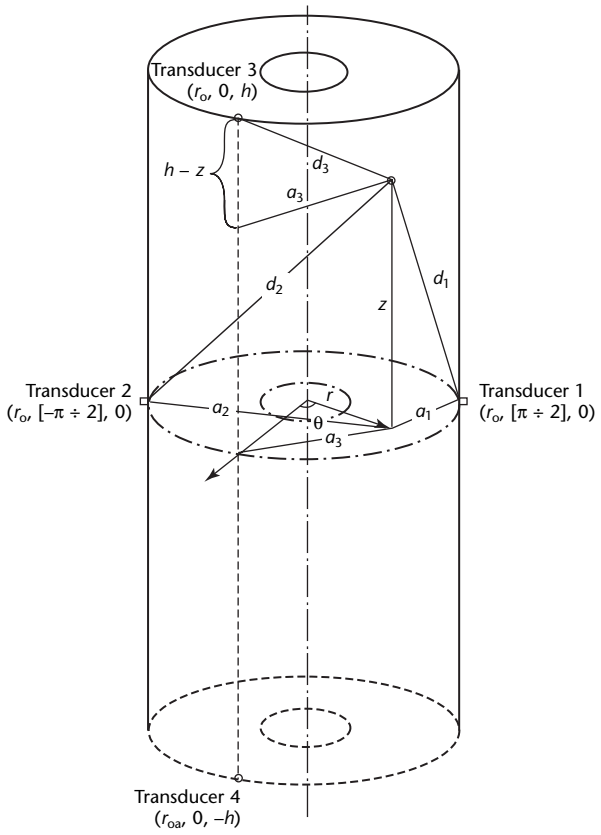

Legend

a_1, a_2, a_3 = horizontal distance (meter) from source to transducers 1, 2 and 3, respectively
d_1, d_2, d_3 = direct distance (meter) from source to transducers 1, 2 and 3, respectively
h = vertical length or height (meter) of cylinder in z direction
r = cylindrical coordinate for radius (meter)
z = cylindrical coordinate for vertical distance (meter)
θ = cylindrical coordinate for angular distance (radian)

be obtained from two loops in a computer program. The radius r varies from the inner radius to the outer radius and the angle θ varies from $(-\pi \div 2)$ to $(\pi \div 2)$. Each loop only needs a limited number of steps to achieve sufficient spatial resolution.

After all solutions for a given θt_{ij} for each pair of transducers are calculated using either Eq. 23 or 24, then a common solution for at least three pairs of transducers can be found by comparing all possible solutions of one pair of transducers with the others. This is achieved by an if-statement routine. The common solution is the location of the source.

Conclusions

Techniques have been shown for locating active sources using the data from one or more transducers. For both discrete and continuous signals, signal difference techniques have been shown that rely on an attenuation model to predict source location. All other techniques discussed rely on timing measurements and work on the assumption that there is one velocity that characterizes wave propagation between two transducers. The remaining discussion expands on the techniques presented above and introduces the concept of propagation of multiple wave modes with different velocities.

PART 2. Overdetermined Source Location

The basis for source location calculations is the time-versus-distance relationship defined by a single characteristic sound velocity. The absolute arrival time t (second) of a hit in an event combined with the velocity v (meter per second) of the sound wave defines the distance d (meter) from the transducer to the source:

$$\textbf{(28)} \quad d = v * t$$

The distance between the source and the transducer that detects it depends on the geometry of the problem. Most of the location modes are a variation of two-dimensional source location in a plane although in many cases the two-dimensional plane will wrap around a three-dimensional object. When the source (at position X_2, Y_2) and transducer (at position X_1, Y_1) are in a flat plane, the distance d between the two is given by the pythagorean theorem expressed in cartesian coordinates:

$$\textbf{(29)} \quad d = \sqrt{(X_2 - X_1)^2 + (Y_2 - Y_1)^2}$$

This calculation is complicated by ignorance of the exact moment the event originated. To get around that problem, all the times are considered relative to the first hit in the event. Each arrival time difference implies a difference in distance to the transducer relative to the distance to the first hit transducer. For the second hit transducer relative to the first hit transducer, a difference equation for arrival times can be written:

$$\textbf{(30)} \quad t_2 - t_1 = \frac{d_2 - d_1}{v}$$

Combining Eqs. 29 and 30 yields:

$$\textbf{(31)} \quad t_2 - t_1 = \left[\sqrt{(X_2 - X_S)^2 + (Y_2 - Y_S)^2} - \sqrt{(X_1 - X_S)^2 + (Y_1 - Y_S)^2}\right] \times v^{-1}$$

where X_S and Y_S are the unknown coordinates of the source. This equation contains two unknowns and cannot be solved by itself. To get a second equation with the same two unknowns, a third hit added to the event produces an analogous equation:

$$\textbf{(32)} \quad t_3 - t_1 = \left[\sqrt{(X_3 - X_S)^2 + (Y_3 - Y_S)^2} - \sqrt{(X_1 - X_S)^2 + (Y_1 - Y_S)^2}\right] \times v^{-1}$$

The complex algebra of these simultaneous equations can then be solved for X_S and Y_S. Most two-dimensional source location algorithms use this approach to produce a source location from the first three hits detected from a given event.

If there are additional hits added to the event, there is a question of how to use the extra information. A better approach would be to average the data somehow to produce a single location.

Multiple regression analysis does this by searching for the location that best fits all the available data. Each additional hit basically adds an extra equation to the set of simultaneous equations given above in Eqs. 31 and 32. This extra equation can be generalized:

$$\textbf{(33)} \quad t_i - t_1 = \left[\sqrt{(X_i - X_S)^2 + (Y_i - Y_S)^2} - \sqrt{(X_1 - X_S)^2 + (Y_1 - Y_S)^2}\right] \times v^{-1}$$

If the difference in arrival time is defined as:

$$\textbf{(34)} \quad \Delta t_i = t_i - t_1$$

then:

$$\Delta t_i = \left[\sqrt{(X_i - X_S)^2 + (Y_i - Y_S)^2} - \sqrt{(X_1 - X_S)^2 + (Y_1 - Y_S)^2}\right] \times v^{-1} \quad (35)$$

Equations 34 and 35 provide two ways of calculating the Δt of the ith transducer. Using the known arrival times of the hits, Eq. 34 can be used to calculate the observed time difference $\Delta t_{i,\text{obs}}$. For a given set of source location coordinates, Eq. 35 defines the calculated time difference $\Delta t_{i,\text{calc}}$. Multiple regression analysis is a general purpose algorithm that minimizes the difference between two quantities, which in this case are the observed and calculated Δt values. To do that, a quantity called *chi squared* (χ^2) is calculated. In this case, χ^2 is defined as the sum across all transducers in the event:

$$\chi^2 = \sum \left(\Delta t_{i,\text{obs}} - \Delta t_{i,\text{calc}}\right)^2 \quad (36)$$

This quantity is also called the *fit value* and depends on the X,Y coordinates of the source position. The sum is recalculated for each potential source location. Assuming no error in the data, χ^2 will have a value of 0 at the source location. The location code searches for the values of X_S and Y_S that minimize the value of χ^2. The process is an iterative search because it is not possible to directly write down simple equations for the values of X_S and Y_S that minimize χ^2.

The search can be performed using a number of standard techniques — for example, using either a simplex search or a powell direction set technique. Multiple regression techniques and search techniques are available for locating a minimum in a function.[6] In particular, detailed information is available elsewhere on simplex and powell searching[7] and on regression analysis.[8]

It is important to note that the regression approach is no longer overdetermined in the case of the event containing the minimum number of hits: three hits for two-dimensional planar location. In that case, however, regression analysis turns out to be mathematically equivalent to solving the complicated algebra of Eqs. 31 and 32 and yields the same location coordinates.

Compressed Gas Cylinder Example

A 470 mm (18.5 in.) diameter compressed gas cylinder was instrumented with nine transducers. Transducers 1, 2 and 3 were mounted around the circumference of the cylinder at the head-to-shell interface and equally spaced. A second ring of transducers numbered 4, 5 and 6 was

FIGURE 13. Two-dimensional source location using three-hit event definition.

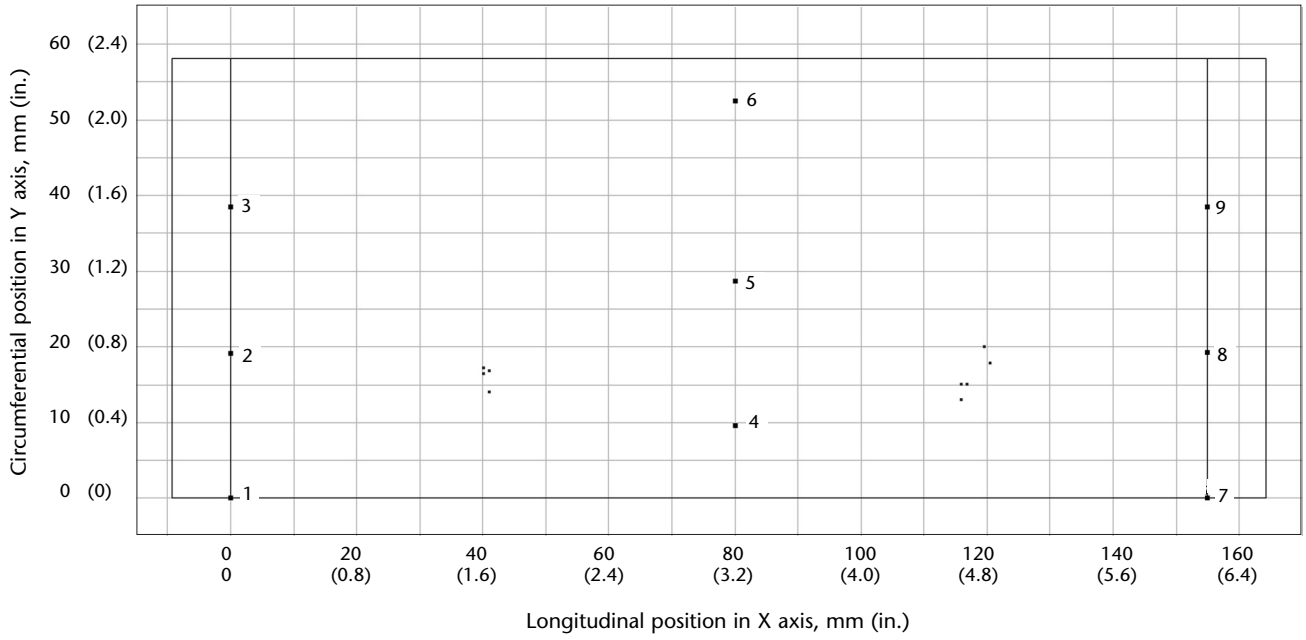

mounted 2 m (80 in.) away in the longitudinal direction and equally spaced around the circumference of the cylinder but offset from the first ring of transducers by 1047 mrad (60 deg). A third ring of transducers numbered 7, 8 and 9 was mounted at the other head-to-shell interface, 3.94 m (155 in.) from the first ring, equally spaced around the circumference and in line with transducers 1, 2 and 3.

A series of 0.3 mm (0.12 in.), hardness 2, pencil graphite breaks, sometimes called pencil lead breaks (PLBs), were performed starting 250 mm (10 in.) away from the first ring of transducers and then every 125 mm (5 in.) after that to 3.5 m (140 in.) from the first ring of transducers. Two-dimensional source location was performed, restricting the event definition to only the first three hits detected. The results are shown in Fig. 13, where the cylinder is sliced open and laid flat for graphical presentation of the source location analysis. Nine transducers are shown numbered. The X axis represents the longitudinal axis of the cylinder and the Y axis represents the circumferential direction. Event positions are shown as dots.

The pencil graphite breaks were performed along a line between transducers 2 and 8. The results are not very good: out of 94 pencil graphite breaks only 14 can be mapped (nine are visible in Fig. 13).

The overall error in the source location analysis is caused by two problems. One is the error in the timing measurements and the other is the problem associated with restricting the event definition to just the first three arriving hits. Pencil graphite breaks executed close to the first ring of transducers will be detected first by the ring of transducers including 1, 2 and 3. These three transducers are all in one plane, making it difficult to calculate a source position even if the timing measurement has no error or very small error.

This restriction was relaxed by allowing the source location algorithm to use four hits to calculate the pencil graphite break position. The results of this exercise are shown in Fig. 14, where immediate improvement is obvious. All 94 pencil graphite breaks are located for this

FIGURE 14. Two-dimensional source location using four-hit event definition, with same transducer locations as in Fig. 13.

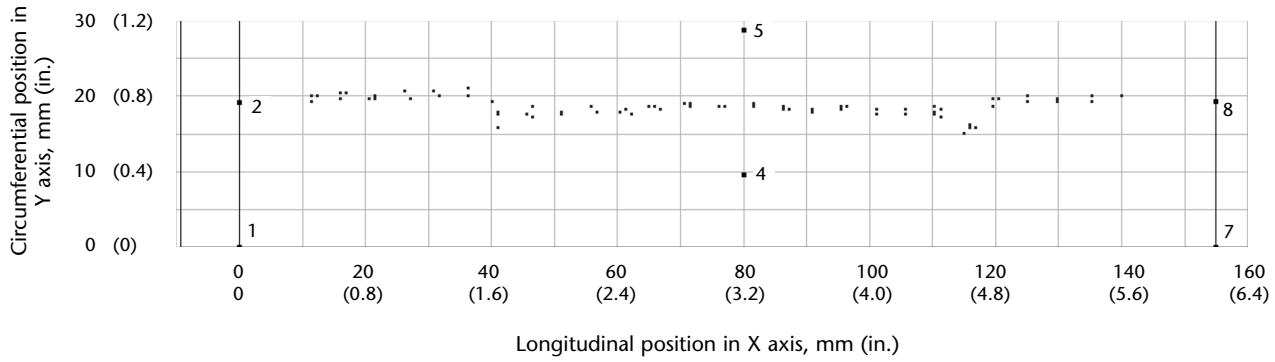

FIGURE 15. Two-dimensional source location using eight-hit event definition, with same transducer locations as in Fig. 13.

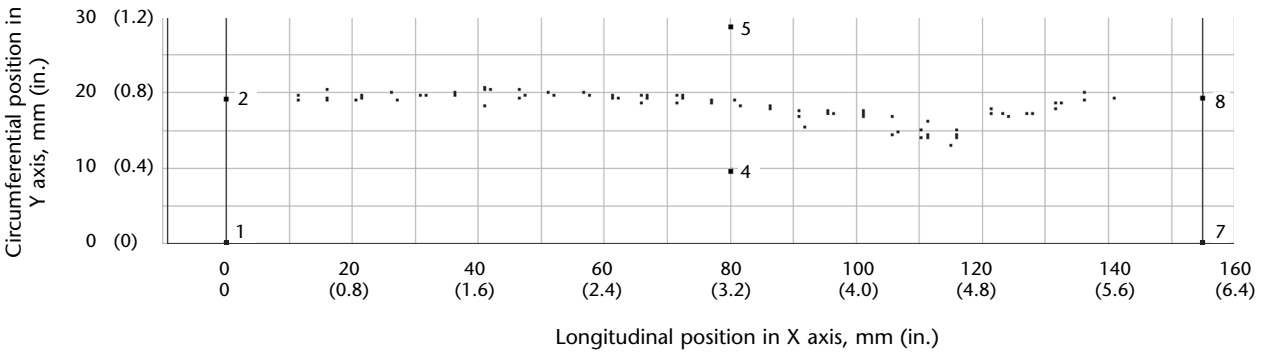

FIGURE 16. Two-dimensional source location using six-hit event definition, with same transducer locations as in Fig. 13.

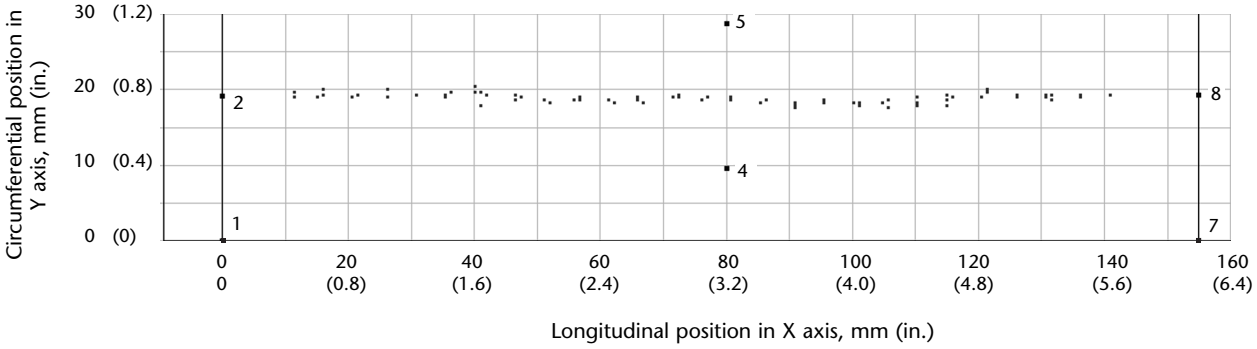

example where the fourth hit is coming from one of the transducers in the second ring of transducers (consisting of 4, 5 and 6) and relieving the problem associated with all of the hits that define the event being in one plane.

A common reaction would be to use all of the hits that are available for the overdetermined source location calculation. In this case, the software has a limit of eight hits. The results of using eight hits to calculate the pencil graphite break locations are shown in Fig. 15. In this case, all 94 pencil graphite breaks are located but the source positions are not as accurate as those in Fig. 14.

The greatest location error is for those events that were generated in the first 1.0 m (40 in.) and the last 1.0 m (40 in.) along the X axis. In these cases, the seventh and eighth hits are coming from the other end of the cylinder where the stress wave generated by the pencil graphite break experiences considerable attenuation to the point where detection may be caused by a different wave mode than those detected by the first six transducers. This attenuation means that the seventh and eighth hits contain considerable timing measurement error compared with the first six hits. Instead of helping, the averaging effect increases the source location error. In fact, for this example, the best setup is to use only the first six hits as shown in Fig. 16.

PART 3. Waveform Based Source Location

A sampling of digital waveforms associated with various hits can be analyzed along with the conventional hit features recorded during a test. Information can be extracted from these waveforms to help locate active sources.

In plate and shell structures, sources are located by reviewing the different wave modes that propagate within a structure. For example, Fig. 17 shows the lamb wave dispersion curves for group velocities in a carbon steel plate.

It can be seen that below 2 mm·MHz, only three wave modes can propagate, the first symmetrical mode and the first two asymmetrical modes. At 2 mm·MHz, these three modes all travel at about the same velocity of 3250 m·s^{-1} (7270 mi·h^{-1}). It can also be seen that, between 0 and 0.3 mm·MHz, the first symmetrical mode is nondispersive. The same can be said for the first asymmetric mode between 1.0 and 1.5 mm·MHz. Waveform based source location can be achieved by digital filtering. The technique that can be derived from this selective filtering can be seen in the following example.

Example Using Alloy Steel

A section of Unified Numbering System G43400 nickel chrome molybdenum alloy steel plate was instrumented with three transducers as shown in Fig. 18. Each transducer was attached to a preamplifier with 40 dB gain and 20 kHz to 2 MHz bandpass filtering. The preamplifier was connected to a parallel processing instrument where the acoustic emission signals were recorded and stored for analysis after the test.

Pencil graphite breaks were performed at four positions: A, B, C and D. The

FIGURE 17. Lamb wave dispersion curves for the group velocities in Unified Numbering System J24055 alloy steel casting.

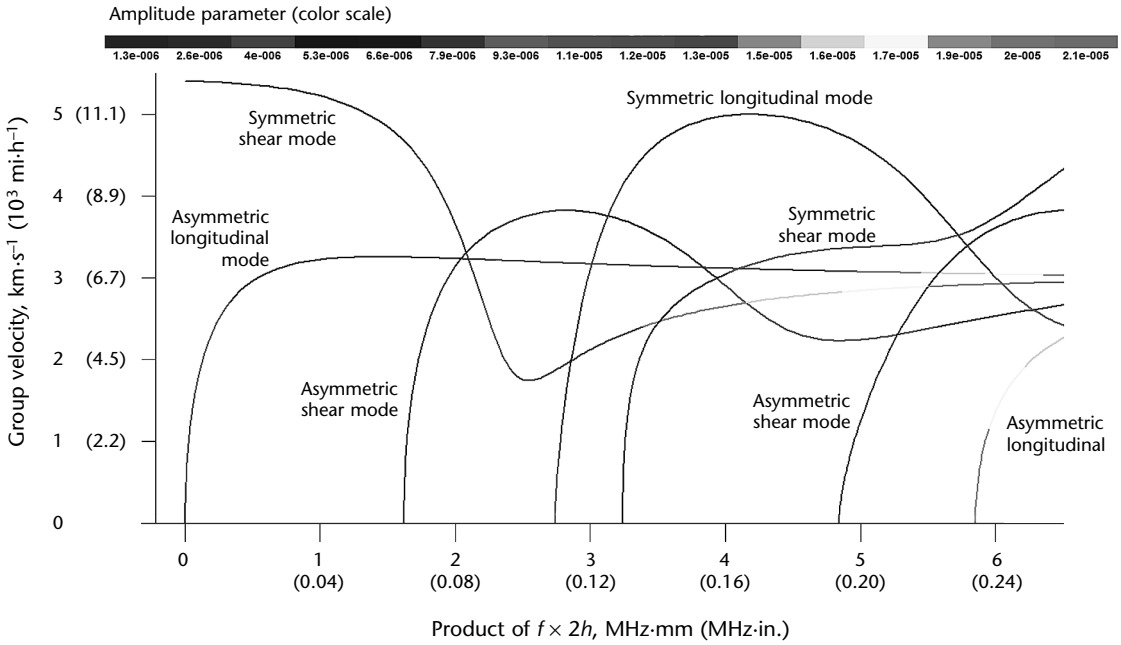

Legend
f = frequency (MHz)
h = vertical distance (mm) to source

coordinates of the transducers and the pencil graphite breaks are given in Table 2.

TABLE 2. Coordinates for transducers and pencil graphite breaks.

Item	*X* Coordinate		*Y* Coordinate	
	m	(in.)	m	(in.)
Transducer 1	0	0	0	0
Transducer 2	0.71	(28)	0	0
Transducer 3	0.28	(11)	0.64	(25)
Position A	0.23	(9)	0.13	(5)
Position B	0.23	(9)	0.38	(15)
Position C	0.41	(16)	0.25	(10)
Position D	0.28	(11)	0.64	(25)

For each position, waveforms were recorded during the pencil graphite breaks. These waveforms were sampled at 5 MHz with 500 µs of pretrigger and 5000 records so that there would be 500 µs of recording after triggering. An example of signals from pencil graphite breakage are shown in Fig. 19, which shows the corresponding waveforms detected at each transducer using a 40 dB detection threshold.

Review of Dispersion Curves

After the pencil graphite break data were recorded and stored, a review of the lamb wave dispersion curves was performed.

FIGURE 18. Transducer and pencil graphite break locations for waveform based source location study.

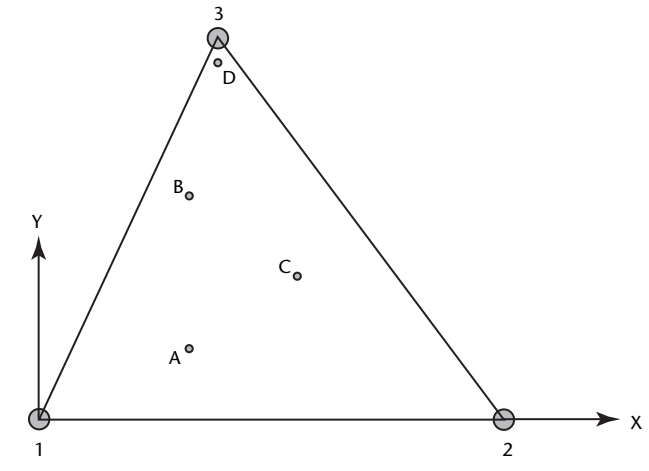

Legend
A, B, C, D = pencil graphite break locations
X, Y = cartesian axes
1, 2, 3 = transducer locations

Because the G43400 plate was 16.5 mm (0.65 in.) thick, the dispersion curves (see Fig. 20) were calculated for this thickness so that specific frequency bands could be identified. Fig. 20 is limited to 200 kHz on the X axis but it may be possible to use higher frequency modes to perform waveform based source location, discussed below.

Triple Point Filtering

Figure 20 shows that all three wave modes propagate at about the same speed (3250 m·s^{-1} [7270 mi·h^{-1}]) near 125 kHz. Based on closer review, a digital bandpass filter from 124 to 127 kHz was used to process the waveforms captured during the pencil graphite breaks at position A.

Each waveform was passed through the digital filter and then compared to a new detection threshold, in this case 25 dB. The detection threshold is lower because the narrow band digital filtering reduces

FIGURE 19. Conventional two-dimensional source location for pencil graphite breaks at position A in Fig. 18: (a) waveforms; (b) plot.

(a)

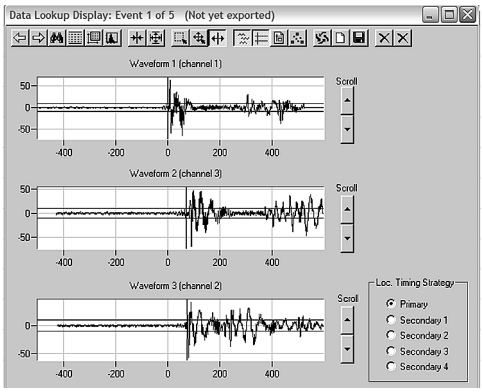

(b)

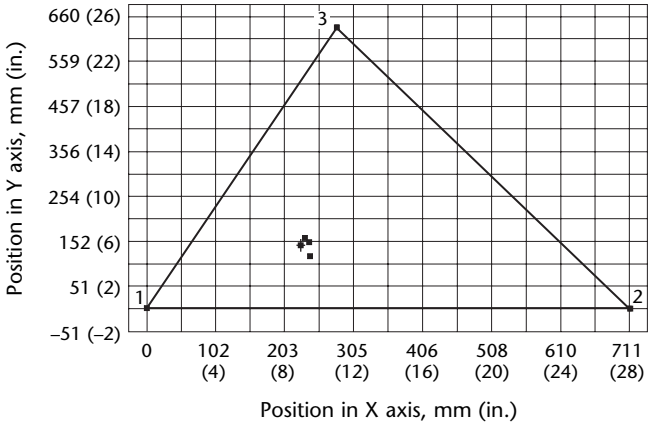

FIGURE 20. Lamb wave dispersion curves of carbon steel plate thickness of 16.5 mm (0.65 in.).

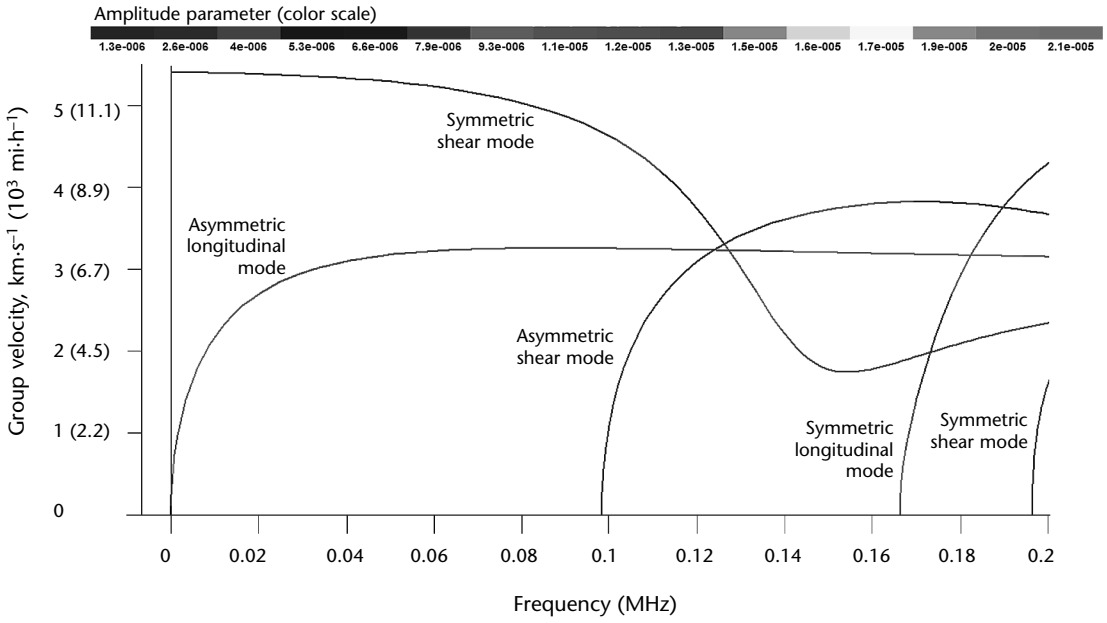

FIGURE 21. Screen display for source location using digitally filtered waveforms at the triple point: (a) waveforms; (b) plot.

(a)

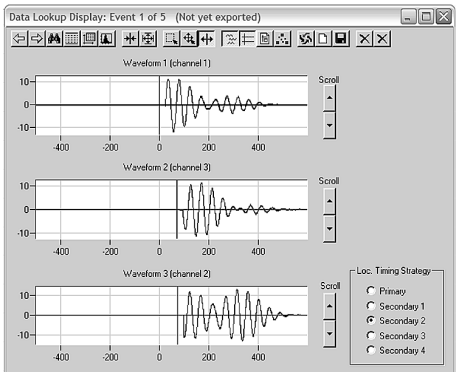

(b)

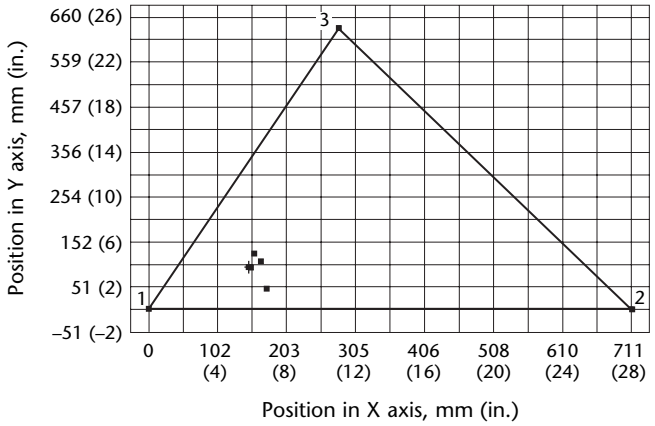

the signal amplitude. The results of the source location from the new timing measurements are shown in Fig. 21, showing improvement over the conventional results shown in Fig. 19. It should also be noted how much the digital filtering reduces the background noise in the signal.

First Motion Detection

Between 20 and 25 kHz, the first symmetric wave mode is nondispersive (see Fig. 20), traveling at a wave speed of 5380 m·s^{-1} (12 035 mi·h^{-1}), almost twice as fast as the fundamental asymmetric mode that propagates in that frequency range. By selectively filtering waveforms at this frequency, it is possible to identify the arrival of the symmetric mode as the first motion in the signal.

The results are shown in Fig. 22, with one example using the set of waveforms (after filtering) for the first three hits. The results compare well with the known position of the source (A), with as much as 125 mm (5.0 in.) in error.

When the front end of the waveforms is expanded, it can be shown that background noise is not completely removed by filtering. Background noise causes triggering at the wrong moment and so causes timing measurement errors that lead to poor location positions.

Asymmetric Wave Mode over Nondispersive Frequency Band

Over the frequency band of 80 to 90 kHz (see Fig. 20), the fundamental asymmetric wave mode is nondispersive whereas the fundamental symmetric mode is not. The wave speed of the asymmetric mode is about 3260 m·s^{-1} (7300 mi·h^{-1}) over this frequency band.

Digitally filtering waveforms over this bandwidth produces the new waveforms and source positions shown in Fig. 23. These show the best results to date with good location accuracy and tight clustering of all five pencil graphite breaks that were recorded.

Conclusion

Waveform based source location shows good potential for accurate source location. Not all techniques work perfectly, as shown above, and there usually is a good explanation if a technique does not work.

The discussion below of source characterization takes this technique a step further by looking at the source-to-receiver distance as it relates to theory. Lamb wave dispersion curves are calculated for the specific plate thickness and source-to-receiver distance so that the source characteristics can be predicted and the source type identified.

FIGURE 22. Screen display for first motion detection after digitally filtering between 20 and 25 kHz: (a) waveforms; (b) plot.

(a)

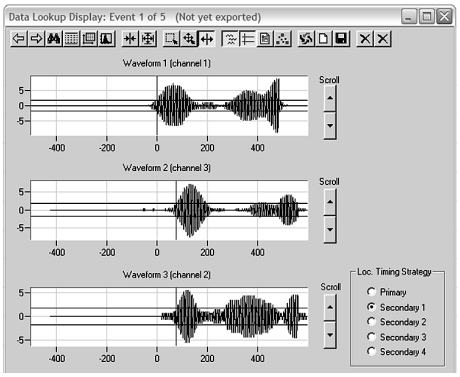

(b)

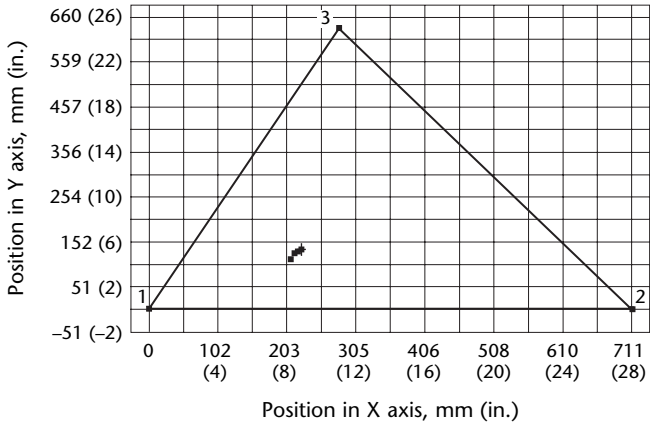

FIGURE 23. Screen display for digital filtering and triggering off of the nondispersive, fundamental asymmetric wave mode: (a) waveforms; (b) plot.

(a)

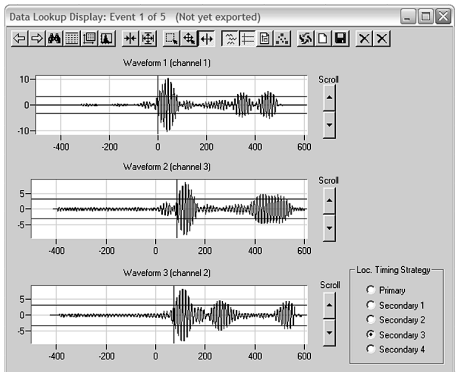

(b)

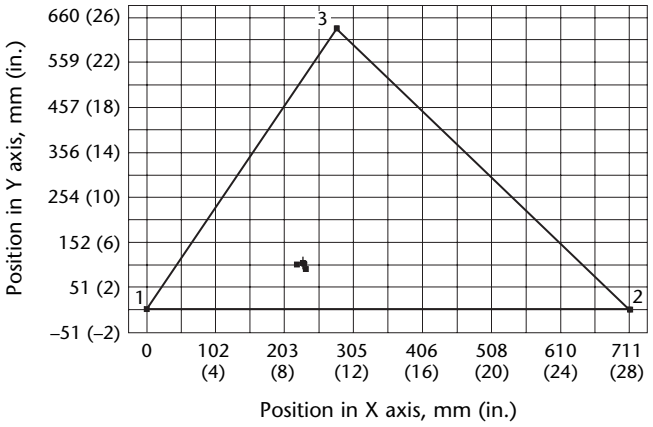

Part 4. Source Location and Characterization Using Lamb Wave Dispersion Curves

Crack detection, identification and location are critical for pressure equipment integrity management in the petroleum industry where acoustic emission testing has been actively used for monitoring crack formation and growth. Weaver and Pao proposed a way to characterize crack emission in a plate using a single waveform.[9] This approach was further developed to determine crack types and source-to-receiver distances as derived from single acoustic emission waveforms. The results of this project are presented below.

Technique

In the far field, the characteristics of an acoustic emission signal generated by a crack in steel plate can be uniquely determined by its densities at 13 mode pair positions on a spectrogram map.[10] A database was built to tabulate the spectrogram density values for the most common source types at plate positions from 0.5 (middle point) up to 1.0 (surface) at these 13 mode pair positions.

In the technique, source identification was achieved by comparing the spectrogram density of the unknown type against the database; the best fitting source type with the highest fitting score (the lowest badness score) was chosen as the source type. The mode with zero frequency on the first symmetric branch and the high frequency modes on the first symmetric and antisymmetric branches were used to determine source-to-receiver distance and to fit the spectrogram to the theoretical dispersion curves.

There are three steps in identifying the source type.

1. The source-to-receiver distance is determined from the waveform by extracting the first time of arrival and the time of rayleigh wave arrival from the waveform or spectrogram and then by using the greatest group velocity in steel to calculate the distance.
2. Fitting of spectrogram and dispersion curves takes place during the refining of the two time-of-arrival values.
3. The last step involves assignment for spectrogram density and solving for the best source type.

Figure 24 shows a spectrogram of a theoretical double force surface source on a 10 mm (0.4 in.) metal plate. Overlaid on the spectrogram are theoretical dispersion curves for the steel plate.

Figure 25a shows the top 16 possible source types and Fig. 25b shows the statistical fitting factor for the 16 solutions. The first solution has the lowest badness score, 0.065, so it is chosen as the most likely source type. It indeed is the source used to generate the spectrogram in the source identification software.

Experimental Evaluation

To study the experimental mode pairs, spectrograms from six types of acoustic emission transducers (Table 3) were studied.

1. Type 1 is a broadband displacement transducer (Fig. 26 and Table 4).
2. Type 2 has a peak resonance of 150 kHz and an integral preamplifier (Fig. 27 and Table 4).
3. Type 3 has a peak resonance of 150 kHz but no integral preamplifier (Fig. 28).
4. Type 4 is a 500 kHz resonant transducer (Fig. 29 and Table 4).

Figure 24. Spectrogram from a theoretical double force surface source. Overlaid is theoretical dispersion curve for a 10 mm (0.4 in.) carbon steel plate.

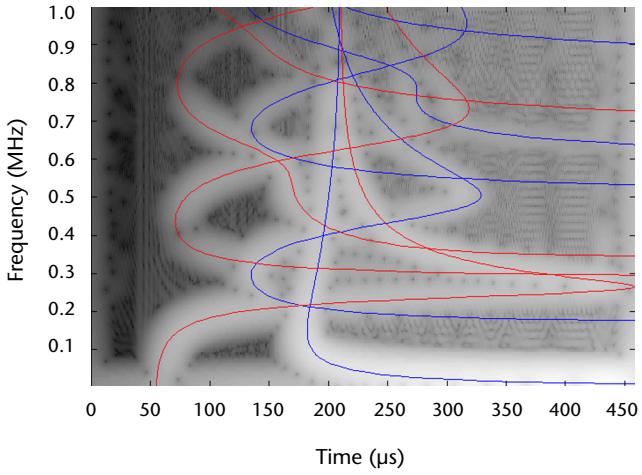

5. Type 5 is a wideband differential transducer having an integral preamplifier (Fig. 30).
6. Type 6 is a resonant transducer having a small aperture and a high frequency range (Fig. 31).

For each transducer type, high pass filters of 20 kHz and 100 kHz were investigated. The pencil graphite break waveforms using the six transducer types were collected on a 16.5 mm (0.65 in.) thick pressure vessel with 5 MHz sampling rate and sample length of 4000 records.

The waveforms analyzed were captured by using data acquisition software. The pretrigger time was set at 100 µs. Figure 32 shows a typical experimental

FIGURE 25. Source type solutions from source identification software: (a) top 16 solutions; (b) statistical fitting factors for the top 16 solutions.

(a)

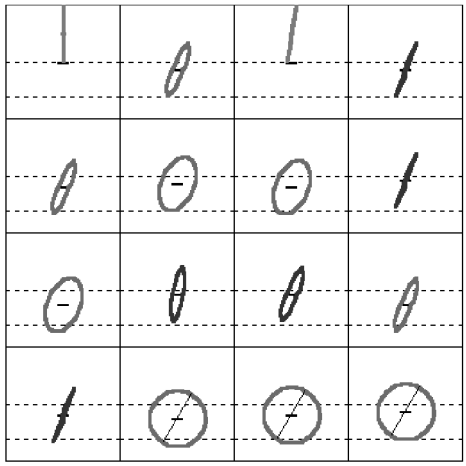

(b)

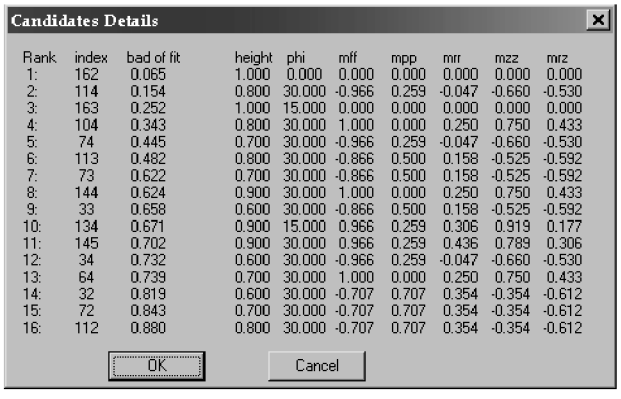

Legend

height = vertical distance, normalized
mff, mpp, mrr, mzz, mrz = moment tensor coordinates
phi = tilt (deg)

TABLE 3. Transducers for studying lamb wave dispersion curves.

Transducer Type	Operating Frequency (kHz)	Peak Resonance (kHz)	Preamplifier	See Figure
1	20 to 1000	500	external	27
2	70 to 200	150	integral	28
3	50 to 200	150	external	29
4	100 to 700	500	external	30
5	100 to 1000	500	integral	31
6	200 to 750	500	external	32

FIGURE 26. Spectrograms from the broadband displacement transducer waveforms: (a) with a 20 kHz high pass filter; (b) with a 100 kHz high pass filter. The white dots indicate locations where mode strength is calculated. The white lines show the mode pairs used to calculate the ratios.

(a)

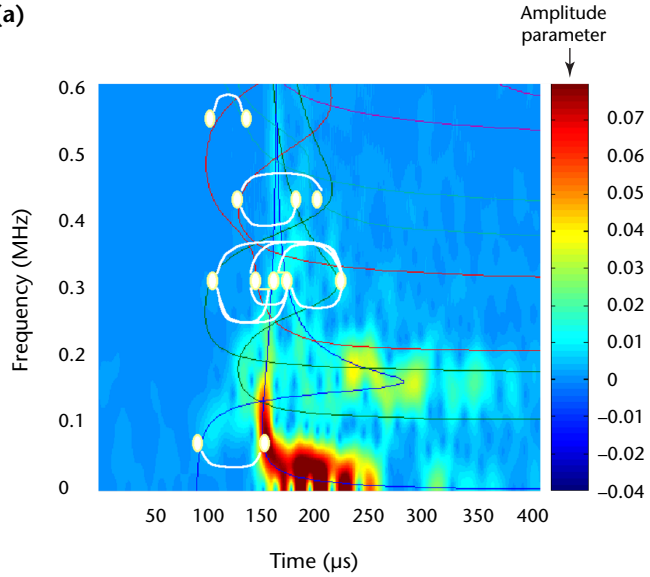

(b)

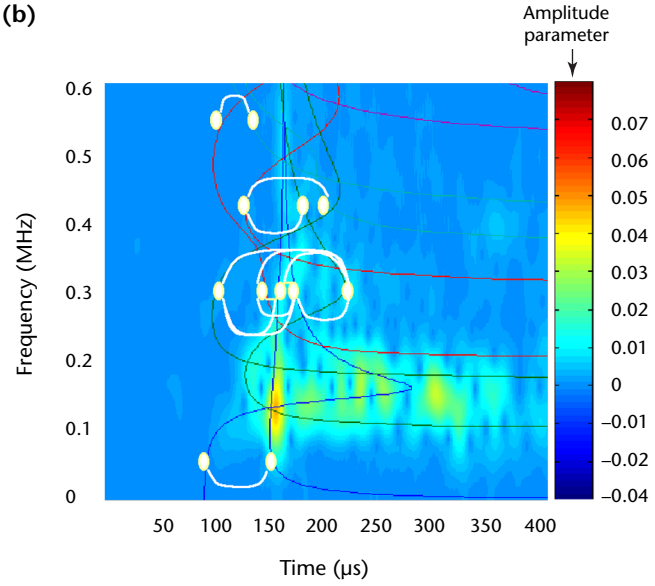

waveform recorded with transducer type 2, having a peak resonance of 150 kHz and an integral preamplifier (Fig. 27), 500 mm (20 in.) from the source on a 16.5 mm (0.65 in.) thick steel plate. The first time of arrival (TOA_1) and the rayleigh time of arrival (TOA_2) were estimated from the waveform and later refined by using the best fitting between spectrogram and theoretical dispersion curves.

The source-to-receiver distance r (meter) is calculated according to Eq. 37:

$$r = \frac{V_1 \times V_2}{V_1 - V_2}\left(\mathrm{TOA}_2 - \mathrm{TOA}_1\right) \quad (37)$$

where V_1 is the first symmetric branch mode group velocity, V_2 is the rayleigh wave group velocity and TOA_2 and TOA_1 are times of arrival for these wave modes.

The spectrograms from waveforms with a 20 kHz high pass and a 100 kHz high pass for each transducer type are plotted in Figs. 26 to 31. Overlaid on the spectrograms are the positions of the time-versus-frequency ranges that define the 13 mode pairs. The spectrograms from transducer types 1, 2 and 3 show that the dominant energy distribution lies between 20 and 250 kHz. When a higher high pass filter is used, such as 100 kHz, the energy distribution moves toward higher frequency modes. However, a higher high pass filter would not significantly change the energy distribution among modes over 250 kHz. By comparing the positions of the preset regions for mode strength calculation and the high energy densities,

TABLE 4. The top nine solutions for pencil break waveforms with 5 MHz sampling rate and 16.5 mm (0.65 in.) plate thickness.

Solution	Badness of Fit	Height (normalized)	Phase ϕ rad	Phase ϕ (deg)	Moment Tensor Coordinates M_{ff}	M_{pp}	M_{rr}	M_{zz}	M_{rz}
Transducer type 1 (displacement transducer) (see Fig. 26)									
1	0.2957	0.7	0.52	(30)	0	1	0.75	0.25	–0.433
2	0.3082	0.7	0.52	(30)	–0.2588	0.9659	0.6597	0.0474	–0.5303
3	0.4010	0.8	0.52	(30)	–0.5	0.866	0.5245	–0.1585	–0.5915
4	0.4017	0.8	0.52	(30)	–0.2588	0.9659	0.6597	0.0474	–0.5303
5	0.4039	0.7	0.52	(30)	–0.5	0.866	0.5245	–0.1585	–0.5915
6	0.4220	0.8	0.52	(30)	0	1	0.75	0.25	–0.433
7	0.4328	0.9	0.26	(15)	0.9659	0.2588	0.3062	0.9186	0.1768
8[a]	0.4340	1.0	0.52	(30)	0	0	0	0	0
9	0.4445	1.0	0.79	(45)	0	0	0	0	0
Transducer type 2 (see Fig. 27)									
1	0.8424	0.6	0.52	(30)	0.2588	0.9659	0.7891	0.4356	–0.3062
2	0.9368	0.6	0.52	(30)	0.0000	1.0000	0.7500	0.2500	–0.4330
3	1.1635	0.7	0.52	(30)	0.2588	0.9659	0.7891	0.4356	–0.3062
4	1.2269	0.7	0.52	(30)	0.8660	0.5000	0.5915	0.7745	0.1585
5	1.2307	0.6	0.52	(30)	0.8660	0.5000	0.5915	0.7745	0.1585
6	1.3909	0.7	0.52	(30)	0.0000	1.0000	0.7500	0.2500	–0.4330
7	1.3962	0.6	0.52	(30)	–0.2588	0.9659	0.6597	0.0474	–0.5303
8	1.4014	0.8	0.52	(30)	0.8660	0.5000	0.5915	0.7745	0.1585
9	1.4090	0.7	0.52	(30)	0.5000	0.8660	0.7745	0.5915	–0.1585
Transducer type 4 (see Fig. 29)									
1	0.5868	0.8	0.52	(30)	0.866	0.5	0.5915	0.7745	0.1585
2	0.6822	0.9	0.52	(30)	0.866	0.5	0.5915	0.7745	0.1585
3	0.7127	0.6	0.52	(30)	–0.2588	0.9659	0.6597	0.0474	–0.5303
4[a]	0.7164	1.0	0.52	(30)	0	0	0	0	0
5	0.7456	0.6	0.52	(30)	–0.5	0.866	0.5245	–0.1585	–0.5915
6	0.7586	0.9	0.26	(15)	0.866	0.5	0.5245	0.8415	0.0915
7	0.7844	1.0	0.79	(45)	0	0	0	0	0
8	0.7885	0.7	0.52	(30)	0	1	0.75	0.25	–0.433
9	0.8135	0.6	0.52	(30)	0	1	0.75	0.25	–0.433

a. Correct source type.

it is found that all 13 pairs except for one are outside the high energy distribution range. This observation is true for the three transducers shown in Figs. 26 to 28.

The spectrograms from transducer types 4 to 6 show that the energy distributes in a wider frequency range, from 50 kHz to 600 kHz. However, in order for all the modes to be accountable, both modes in a mode pair have to be present. As shown in Figs. 29 to 31, most of the mode pairs have only one strong mode. The lack of one mode renders the pair useless for identifying the source type.

In summary, the experimental waveform analysis shows that the mode pairs used in the algorithm are outside the frequency range in which the experimental waveforms carry significant energy. Therefore, to use this approach effectively, it is necessary to revise the location of the wave mode pairs by using the appropriate frequency ranges as depicted in Figs. 26 to 31.

FIGURE 27. Spectrograms of waveforms from a transducer having peak resonance of 150 kHz, with an integral preamplifier: (a) with a 20 kHz high pass filter; (b) with a 100 kHz high pass filter. The white dots indicate locations where mode strength is calculated. The white lines show the mode pairs used to calculate the ratios.

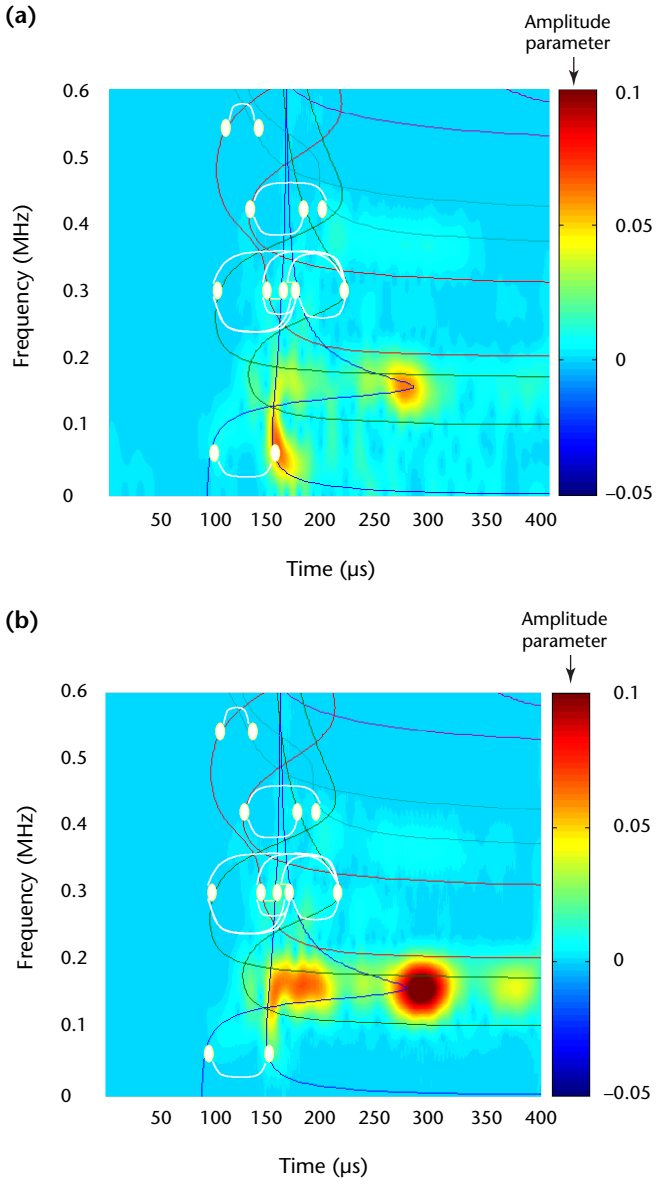

FIGURE 28. Spectrograms of waveforms from the transducer having peak resonance of 150 kHz but no integral preamplifier: (a) with a 20 kHz high pass filter; (b) with a 100 kHz high pass filter. The white dots indicate locations where mode strength is calculated. The white lines show the mode pairs used to calculate the ratios.

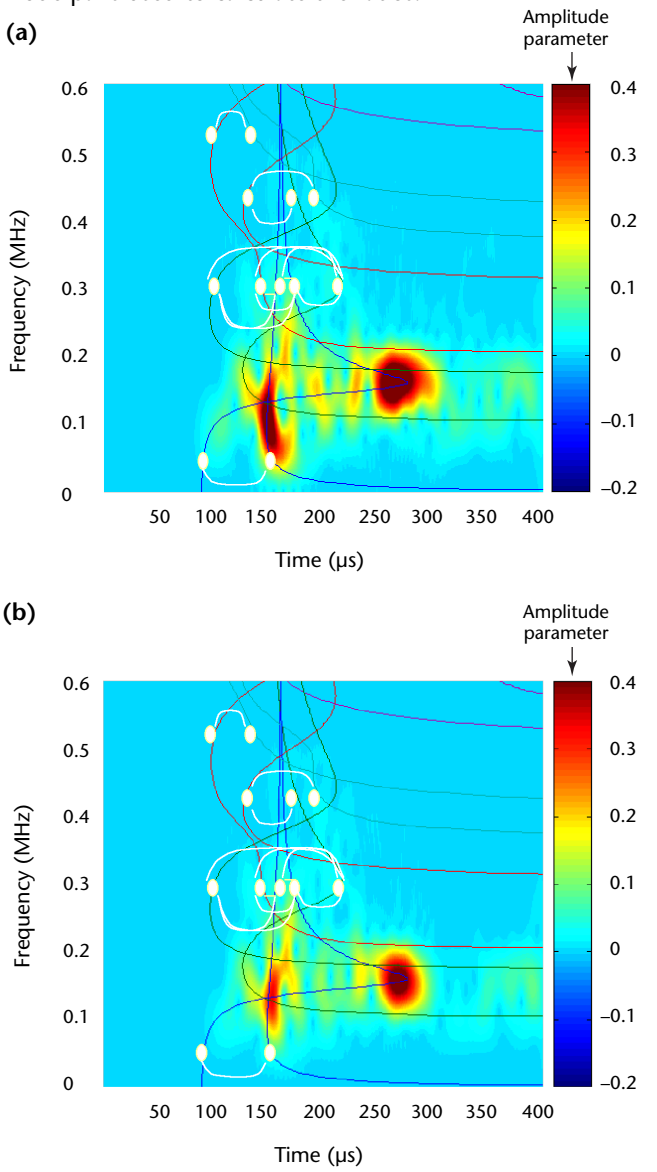

Source Identification Using Pencil Break Waveforms

Pencil break waveforms from transducer types 1 to 6 were evaluated with the source identification software. Figure 33 shows the top nine source type candidates for each of the six types of transducers determined by the software. The source types are described by their moment tensor plots. The horizontal blank line in the figures shows the source height in the plate; the vertical pink line denotes step surface forces. In the current version, all surface forces, including vertical and oblique, are presented by the same vertical line. Modifications can permit tilted lines to represent oblique surface step forces according to the value of the angle.

It is known that a pencil break is best described as a surface oblique step force with an angle of about 0.5 rad (30 deg). Figure 33 shows that the correct source type for the pencil break is among the top nine selected for transducer types 1 and 4 but not for other transducers. A common feature for all transducer types is that all of the source type candidates are oblique forces but at different heights. A detailed description of the top nine source type candidates is shown in Table 4 for transducer types 1, 2 and 4.

FIGURE 29. Spectrograms from a 500 kHz resonant transducer: (a) with a 20 kHz high pass filter; (b) with a 100 kHz high pass filter. The white dots indicate locations where mode strength is calculated. The white lines show the mode airs used to calculate the ratios.

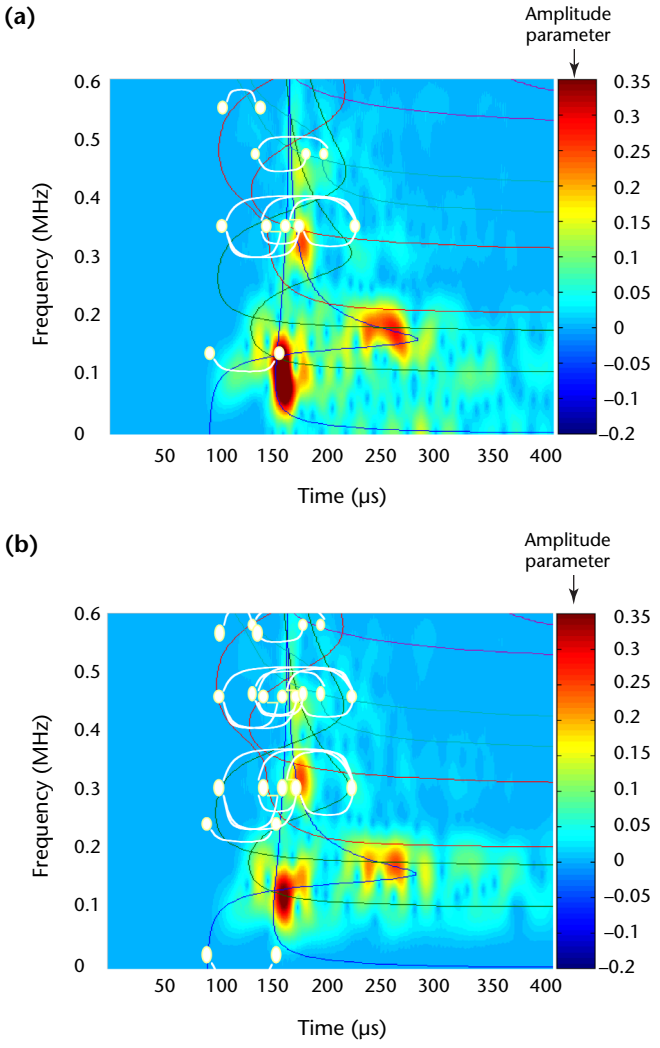

FIGURE 30. Spectrograms of waveforms from a wideband differential transducer: (a) with a 20 kHz high pass filter; (b) with a 100 kHz high pass filter. The white dots indicate locations where mode strength is calculated. The white lines show the mode pairs used to calculate the ratios.

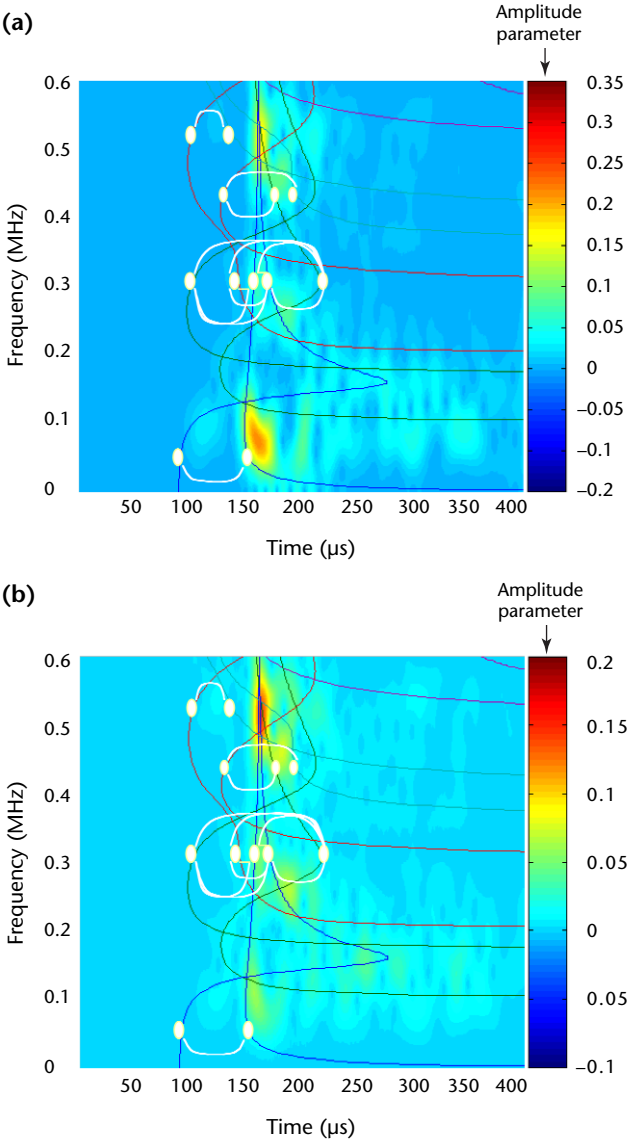

The data in Table 3 further show that most of the candidates have an oblique angle of about 0.5 rad (30 deg) but the normalized height can be 0.6 to 1.0. For transducer type 1, the correct source type is at the eighth position with a badness of fit of 0.43 and the correct source type is at the fourth position with a badness of fit of 0.716 for transducer type 4. These results are not as encouraging as the results obtained with the theoretical waveforms. The broad band and high frequency band transducers (types 1 and 4) seem to render better results than do the narrow band transducers, type 2. Transducers with and without internal amplifiers give the same results. This indicates that internal and external amplifiers do not affect source identification.

It is concluded that the source identification procedure is not as accurate on experimental data as on theoretical data. One reason can be that the predetermined time-versus-frequency ranges for mode strength calculations are in general weak in an experimental spectrogram and the strong experimental modes are not included in the calculation.

Although the source identification procedure failed to select the correct source type, it was very good at determining the source start time and the source-to-receiver distance for pencil break data. The average error for the source-to-receiver distance is one percent.

The top nine source type candidates for pencil break[11,12] waveforms were recorded with six different transducer types. The source types are characterized by their moment tensor diagrams.

FIGURE 31. Spectrograms of waveforms from a resonant transducer having a small aperture and high frequency: (a) with a 20 kHz high pass filter; (b) with a 100 kHz high pass filter. The white dots indicate locations where mode strength is calculated. The white lines show the mode pairs used to calculate the ratios.

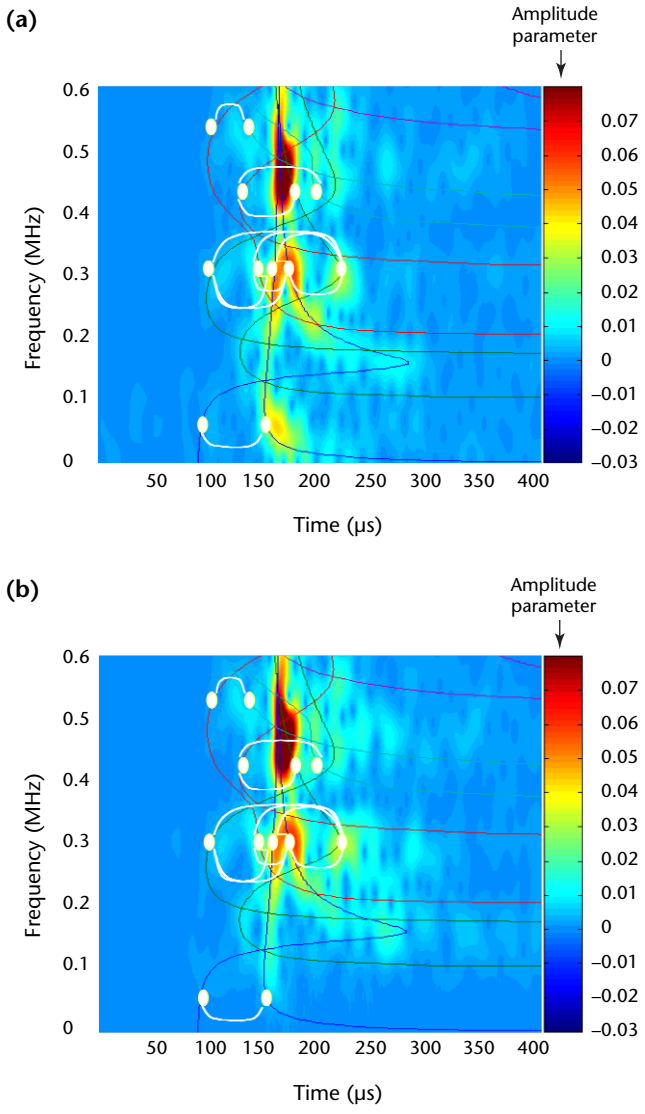

Summary

The single-waveform approach to identifying acoustic emission source types has success with theoretical waveforms but limited success with experimental waveforms. Study of experimental modes with various transducer types shows that the time-versus-frequency ranges used for source identification in the software do

FIGURE 32. Waveform captured with 150 kHz resonant transducer with integral preamplifier at 500 mm (20 in.) from pencil break source. Times of arrival can be estimated from the waveform as illustrated by the arrows.

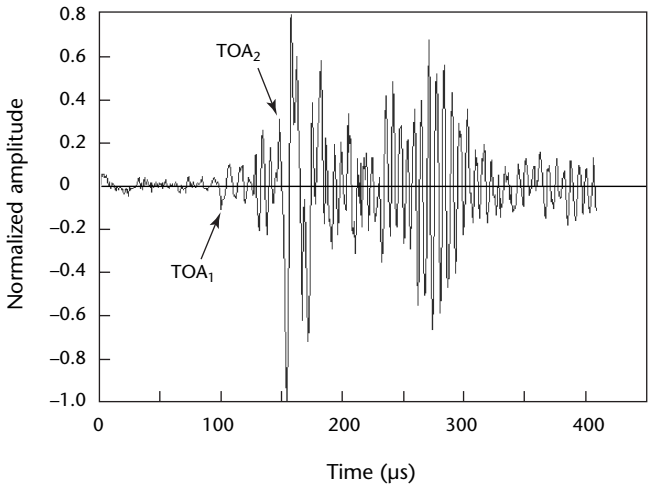

Legend

TOA_1 = first time of arrival
TOA_2 = rayleigh time of arrival

not normally have strong wave modes. On the other hand, the strong modes in experimental spectrograms are mostly not included in the source identification procedure. Redefining the mode pair positions according to the strong modes in experimental spectrograms for a specific transducer type may lead to an effective source identification procedure for experimental data. Although the technique fails to predict the correct source types for pencil break waveforms, it succeeds in calculating the source-to-receiver distances with an approximate error of one percent.

FIGURE 33. Software displays for top nine source type candidates for pencil break waveforms recorded with six different transducer types: (a) type 1, broad band displacement transducer; (b) type 2, transducer having peak resonance of 150 kHz, with an integral preamplifier; (c) type 3, transducer having peak resonance of 150 kHz; (d) type 4, 500 kHz resonant transducer; (e) type 5, wide band resonant transducer; (f) type 6, transducer having a small aperture and 500 kHz resonant transducer. The source types are characterized by their moment tensor diagrams.

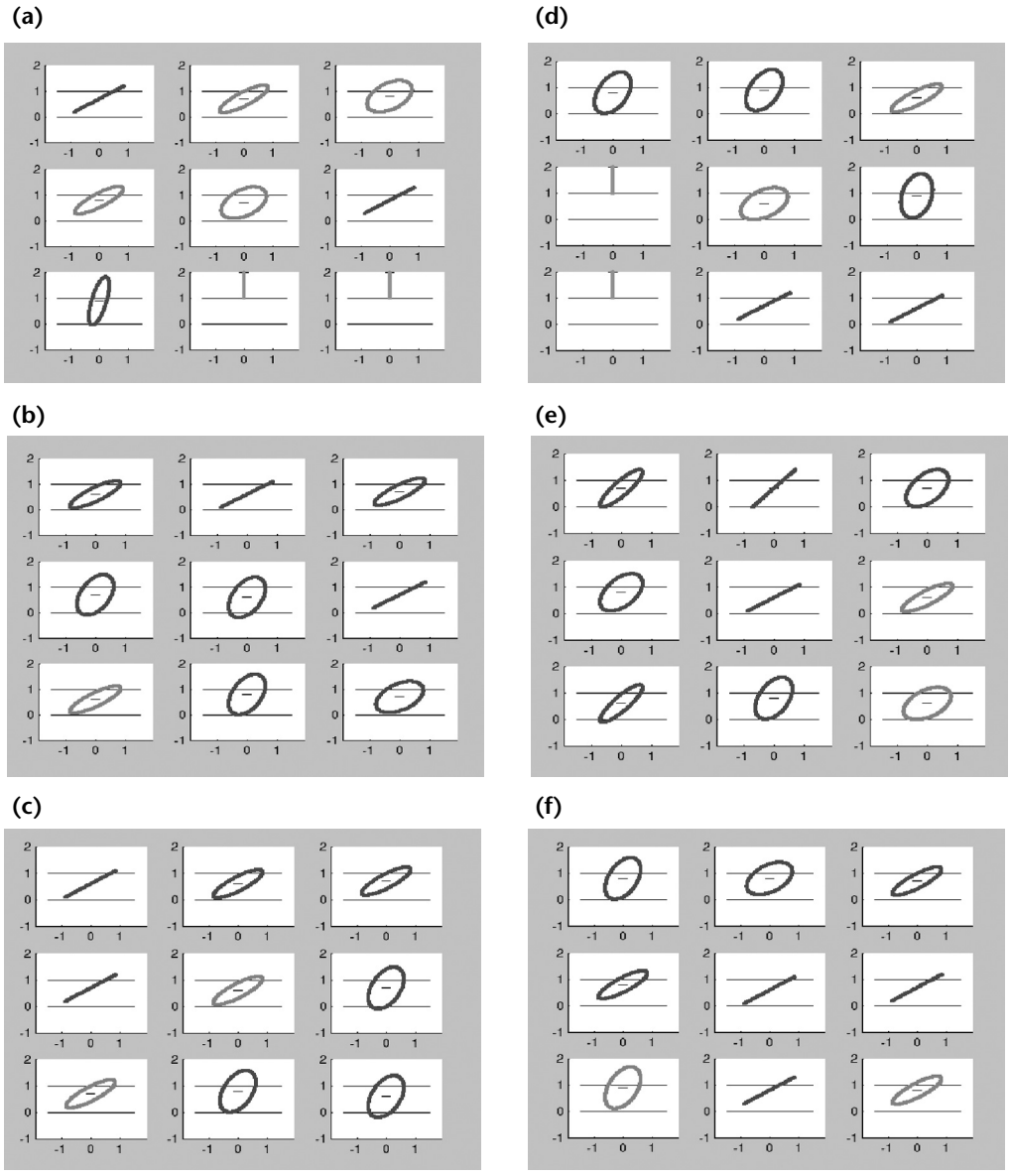

References

1. Baron, J.A. and S.P. Ying. Section 6, "Acoustic Emission Source Location." *Nondestructive Testing Handbook,* second edition: Vol. 5, *Acoustic Emission Testing*. Columbus, OH: American Society for Nondestructive Testing (1987): p 135-154.
2. Kitajima, A. et al. *Acoustic Leak Detection in Piping Systems*. CRIEPI Report 283006. Tokyo, Japan: Central Research Institute of Electric Power Industry (April 1984).
3. Bendat, J.S. and A.G. Piersol. *Engineering Applications of Correlation and Spectral Analysis*. New York, NY: John Wiley and Sons (1980).
4. Tatro, C.A., A.E. Brown, T.H. Freeman and G. Yanes. "On-Line Safety Monitoring of a Large High Pressure High Temperature Autoclave." *Acoustic Emission Monitoring of Pressurized Systems*. Special Technical Publication 697. West Conshohocken, PA: ASTM International (1979): p 70-90.
5. Kupperman, D.S., D. Prine and T. Mathieson. NUREG/CR-5134, *Application of Acoustic Leak Detection Technology for the Detection and Location of Leaks in Light Water Reactors*. Argonne, IL: United States Department of Energy, Argonne National Laboratory (1988).
6. Press, W.H., B.P. Flannery, S.A. Teukolsky and W.V. Vetterling. *Numerical Recipes in C*. London, United Kingdom: Cambridge University Press (1992).
7. Hopwood, T. and C. McGogney. Section 10, "Acoustic Emission Applications in Civil Engineering." *Nondestructive Testing Handbook,* second edition: Vol. 5, *Acoustic Emission Testing*. Columbus, OH: American Society for Nondestructive Testing (1987): p 311-345.
8. Mobley, K., C. Bailey, K. Bierney, H. Berger, M. Goodman, J. Judd, C. Lewis, J. Rogers and S. Slykhous. Section 15, "Survey of Commercial Sensors and Systems for Acoustic Emission Testing." *Nondestructive Testing Handbook,* second edition: Vol. 5, *Acoustic Emission Testing*. Columbus, OH: American Society for Nondestructive Testing (1987): p 513-549.
9. Weaver, R.L. and Y.-H. Pao. "Axisymmetric Elastic Waves Excited by a Point Source in a Plate." *Journal of Applied Mechanics*. Vol. 49, No. 12. New York, NY: ASME International (December 1982): p 821-836.
10. Weaver, R.L. *Theoretical Modeling of Acoustic Emission Wave Propagation in Flat Infinite Plates: Study of the Inverse Problem*. Princeton, NJ: Physical Acoustics Corporation (2001).
11. Hsu, N.N. *Acoustic Emission Simulator.* United States Patent 4018084 (April 1977).
12. Nielsen, A. *Acoustic Emission Source Based on Pencil Lead Breaking*. Copenhagen, Denmark: Danish Welding Institute (1980).